HHS Public Access

Author manuscript

Immunity. Author manuscript; available in PMC 2023 February 08.

Published in final edited form as:

Immunity. 2022 February 08; 55(2): 237–253.e8. doi:10.1016/j.immuni.2021.12.016.

IL-17RA-signaling in Lgr5^{+} intestinal stem cells induces expression of transcription factor ATOH1 to promote secretory cell lineage commitment

Xun Lin[1,*], **Stephen J. Gaudino**[1,*], **Kyung Ku Jang**[2,*], **Tej Bahadur**[1], **Ankita Singh**[1], **Anirban Banerjee**[1], **Michael Beaupre**[1], **Timothy Chu**[1], **Hoi Tong Wong**[1], **Chang-Kyung Kim**[3], **Cody Kempen**[1], **Jordan Axelrad**[4], **Huakang Huang**[1], **Saba Khalid**[1], **Vyom Shah**[5], **Onur Eskiocak**[5], **Olivia B. Parks**[6], **Artan Berisha**[1], **Jeremy P. McAleer**[7], **Misty Good**[8], **Miko Hoshino**[9], **Richard Blumberg**[10], **Agnieszka B. Bialkowska**[3], **Sarah L. Gaffen**[11], **Jay K. Kolls**[12], **Vincent W. Yang**[3], **Semir Beyaz**[5], **Ken Cadwell**[2,4,13,$], **Pawan Kumar**[1,#,$,@]

[1] Department of Microbiology and Immunology, Stony Brook University, Stony Brook, NY, United States

[2] Kimmel Center for Biology and Medicine at the Skirball Institute, New York University Grossman School of Medicine, New York, NY, USA

[3]Department of Medicine, Renaissance School of Medicine, Stony Brook University, Stony Brook, NY, 11794, United States

[4] Division of Gastroenterology and Hepatology, Department of Medicine, New York University Grossman School of Medicine, New York, NY 10016, USA.

[5] Cold Spring Harbor Laboratory, Cold Spring Harbor, NY 11724, USA.

[6] University of Pittsburgh School of Medicine, Medical Scientist Training Program, Pittsburgh, PA 15213, USA

[7] Department of Pharmaceutical Science, Marshall University School of Pharmacy, Huntington, WV, 25701, USA

[8] Washington University School of Medicine, Department of Pediatrics, Division of Newborn Medicine, St. Louis Children's Hospital, St. Louis, MO, 63110, USA

[#]Correspondence: Pawan Kumar, **Assistant Professor**, pawan.kumar@stonybrook.edu, Office: 631-632-4242.
[*]These authors contributed equally
[$]Senior author
[@]Lead contact

AUTHOR CONTRIBUTIONS

XL, SJG, PK, KKJ and KC designed the experiments. PK, KC, XL, SJG and KKJ wrote the manuscript. PK, XL, SJG, KS, AB, AS, TB, CK, HTW, AB, MB, and SC performed key experiments and data analyses. TB, CK, and SJG performed organoid cultures, stimulation, and analysis. TB, XL, KKJ, OBP, TC and SJG performed all immunofluorescence staining. XL, SJG and HTW performed alcian blue staining and data analysis. MB, XL, AS and SJG performed all RT-PCR and DSS experiments. AS and XL performed and analyzed all flow cytometry data. JA and KKJ generated and analyzed human-derived samples. MG, AB, VWY, HM and RB provided critical experimental samples. All authors discussed data and commented on the manuscript, including critical revision of the manuscript.

[9] Department of Biochemistry and Cellular Biology, National Institute of Neuroscience, National Center of Neurology and Psychiatry, Kodaira, Tokyo 187-8502, Japan.

[10] Department of Medicine, Brigham and Women's Hospital, Harvard Medical School, Boston, MA, 02115, USA

[11] Division of Rheumatology and Clinical Immunology, School of Medicine, University of Pittsburgh, PA, 15261, USA

[12] Center for Translational Research in Infection and Inflammation Tulane School of Medicine, LA, 70112, USA

[13] Department of Microbiology, New York University Grossman School of Medicine, New York, NY 10016, USA.

SUMMARY

The Th17 cell lineage-defining cytokine IL-17A contributes to host defense and inflammatory disease by coordinating multicellular immune responses. The IL-17 receptor (IL-17RA) is expressed by diverse intestinal cell types, and therapies targeting IL-17A induce adverse intestinal events, suggestive of additional tissue-specific functions. Here, we used multiple conditional deletion models to identify a role for IL-17A in secretory epithelial cell differentiation in the gut. Paneth, tuft, goblet, and enteroendocrine cell numbers were dependent on IL-17A-mediated induction of the transcription factor *Atoh1* in $Lgr5^+$ intestinal epithelial stem cells. Although dispensable at steady state, IL-17RA signaling in $ATOH1^+$ cells was required to regenerate secretory cells following injury. Finally, IL-17A stimulation of human-derived intestinal organoids that were locked into a cystic immature state induced *ATOH1* expression and rescued secretory cell differentiation. Our data suggest that the crosstalk between immune cells and stem cells regulates secretory cell lineage commitment and the integrity of the mucosa.

In Brief:

IL-17A is critical for maintaining intestinal integrity and may play a beneficial role in IBD, but the extent of its tissue-specific roles remains unclear. Lin et al. show that IL-17A acts specifically on $Lgr5^+$ intestinal stem cells to induce *Atoh1* expression and promote differentiation into secretory cells. Furthermore, IL-17A protects against DSS-induced injury through $ATOH1^+$ cell-mediated regeneration of $Lgr5^+$ ISCs.

Graphical Abstract

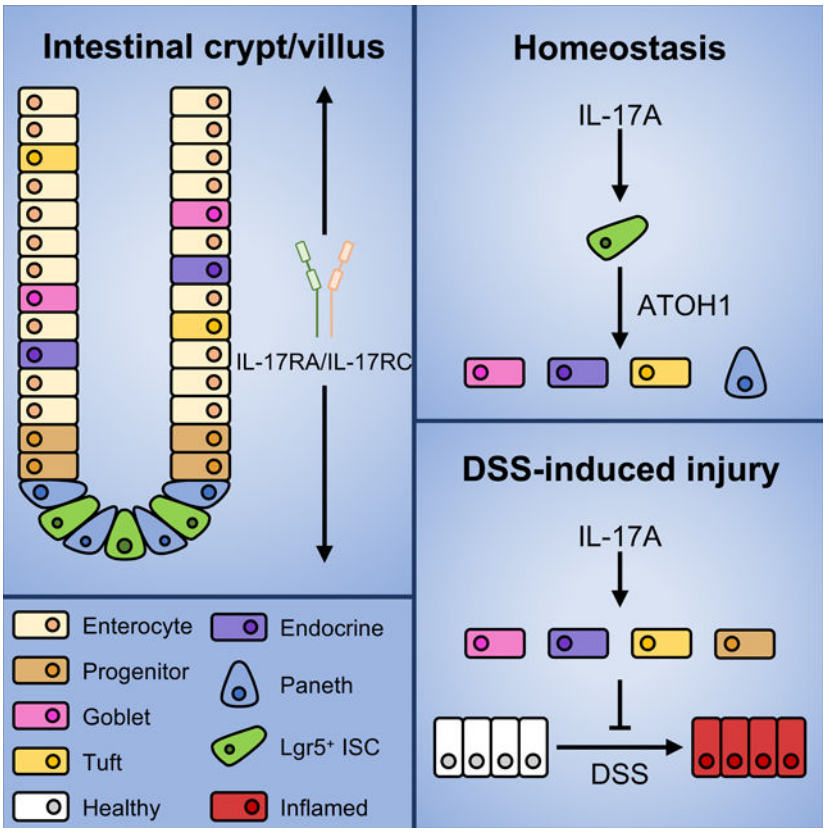

INTRODUCTION

Interleukin (IL)-17A is an inflammatory cytokine that is predominantly produced by Th17 cells and has an established role in coordinating multicellular immunity. IL-17A, along with its close family member IL-17F, is released in response to microbial pathogens. These cytokines signal via the IL-17RA/IL-17RC receptor complex to mediate the recruitment of neutrophils, antimicrobial peptides and other processes critical for host defense (Kumar et al., 2016; Lee et al., 2015; Song et al., 2015). IL-17A responses have also been associated with chronic inflammation and autoimmune diseases. Monoclonal antibodies against IL-17A or IL-17RA have been shown to be highly effective treatments for moderate to severe plaque psoriasis (Gordon et al., 2016; Langley et al., 2014; Papp et al., 2012). However, the same drugs failed to improve Crohn's disease, a type of inflammatory bowel disease, and an alarming number of patients displayed increased adverse events and worsening of intestinal disease (Hueber et al., 2012; Targan et al., 2016). There have even been reports of new onset IBD in individuals receiving therapies targeting IL-17A (Ali et al., 2021; Fauny et al., 2020; Mu et al., 2021), suggesting that IL-17A has an essential homeostatic function in the gut. Consistently, we and others have shown that IL-17A is critical for preserving epithelial barrier function and regulating gut microbiota colonization (Kumar et al., 2016; Lee et al., 2015; Maxwell et al., 2015; Song et al., 2015). Additionally, the colonic epithelium of IBD patients accumulates mutations affecting IL-17A signaling (Nanki et al., 2020). In contrast, IL-17A has also been shown to exacerbate intestinal inflammation and the progression of

colorectal cancer (Hyun et al., 2012; Oshiro et al., 2012; Wang et al., 2014; Wu et al., 2009). Thus, the effects of IL-17A in the intestines are complex, and the tissue-specific function of this cytokine requires further investigation.

The epithelium of the small intestine is comprised of distinct lineages that are organized into crypt-villus projections. $Lgr5^+$ intestinal stem cells (ISCs) reside at the base of the crypt and are interspersed by Paneth cells, a lineage of secretory cells that release antimicrobial peptides and growth factors providing protection against microbial pathogens and promoting a niche for ISC development (Adolph et al., 2013; Ramanan and Cadwell, 2016; Salzman, 2010; Sato et al., 2011b). $Lgr5^+$ cells constitute a major pool of ISCs which gives rise to different intestinal epithelial cell types under homeostatic conditions (Barker and Clevers, 2010). As ISCs proliferate, they move up in the crypt and differentiate into absorptive enterocytes or unique lineages of secretory cells. These secretory lineages include goblet, enteroendocrine and tuft cells. While enteroendocrine cells predominantly secrete regulatory digestive hormones, goblet and tuft cells aid in the protection of the intestinal epithelium.

IL-17A regulates the expression of antimicrobial enterocyte-specific polymeric immunoglobulin receptor (*Pigr*) and Lipocalin 2 (*Lcn2*) (Onishi and Gaffen, 2010; Shen et al., 2006). However, IL-17RA is expressed on all intestinal cell types including progenitor cells and ISCs, raising the possibility that IL-17A signaling contributes to epithelial cell lineage commitment. $Lgr5^+$ ISCs give rise to progenitor cells that express hairy and enhancer of split-1 (HES1) and atonal homolog 1 (ATOH1), transcription factors that regulate intestinal absorptive and secretory epithelial cell differentiation, respectively (Durand et al., 2012). While the role of ATOH1 in regulating Paneth, enteroendocrine and goblet cell lineages is well characterized (Yang et al., 2001), the regulation of tuft cells by ATOH1 is still debatable (Gerbe et al., 2011; Gracz et al., 2018). Recent cell-lineage tracing studies have shown that $ATOH1^+$ cells possess stem cell properties and mediate regeneration of the epithelium following injury (Ishibashi et al., 2018; Tomic et al., 2018). It is unknown whether IL-17A regulates the differentiation and function of ISCs and/or $ATOH1^+$ progenitor cells.

Here, we demonstrate that IL-17A promotes *Atoh1* expression in $Lgr5^+$ ISCs and the differentiation of intestinal epithelial secretory cell lineages. Additionally, inducible deletion of IL-17RA in $ATOH1^+$ cells compromises recovery from intestinal injury. These results identify a role for the IL-17RA-Lgr5-ATOH1 axis in secretory epithelial cell lineage commitment during homeostasis and injury responses.

RESULTS

IL-17A regulates intestinal secretory cell lineage commitment

We first investigated the role of IL-17A in epithelial cell differentiation by using murine small intestinal organoids, a three-dimensional (3D) cell culture system in which enterocytes and secretory epithelial lineages are differentiated from primary crypts in the presence of growth factors (Sato et al., 2009). We found that IL-17A stimulation of small intestinal organoids increased the expression of secretory cell-specific genes *Chga* (enteroendocrine cells), *Muc2* (goblet cells) and *Lyz1* (Paneth cells) but had no effects on enterocyte-specific

genes (*Abop* and *Enpep*) (Figure 1A). Furthermore, immunofluorescence microscopy demonstrated increased numbers of LYZ1^{+} cells and cells bound by UEA1, a lectin that binds secretory granules, in response to IL-17A stimulation (Figure 1B). In contrast, IL-17A treatment for 7 hours was not capable of increasing *Chga, Muc2* and *Lyz1* expression in day 5 differentiated organoids. As a positive control, *Pigr* was induced by IL-17A (Figure 1C). These results are consistent with a role for IL-17A in promoting secretory cell differentiation rather than maturation. Organoid establishment and differentiation depend on a number of growth factors. R-spondin, Wnt and Noggin activate Wnt/Notch signaling for stemness, organoid growth and enterocyte differentiation. In addition, CHIR99021, a GSK3 inhibitor, is added to promote organoid growth (Figure S1A), secretory cell differentiation, stem cell self-renewal, and reduce enterocyte differentiation (Farin et al., 2012; Yin et al., 2014). To determine whether IL-17A activity is dependent on CHIR99021, we excluded CHIR99021 in the organoid culture. As expected, in the absence of CHIR99021, IL-17A had no effect on secretory cells or enterocytes (Figure S1B). These results suggest that IL-17A can promote secretory cell lineage commitment under defined growth conditions.

We next examined the expression of secretory cell-specific genes in the small intestine (ileum) of *Il17ra*$^{-/-}$ mice and intestinal epithelium-specific *Il17ra*-deficient mice (*Il17ra*$^{fl/fl}$*;Villin-cre*). *In vivo*, we observed decreased expression of *Dclk1* (tuft cell), *Chga* (enteroendocrine cell), *Clca1* and *Muc2* (goblet cell) in *Il17ra*$^{fl/fl}$*;Villin-cre*$^{+}$ and *Il17ra*$^{-/-}$ mice when compared to their littermate cre^{-} or wild-type control groups (Figures 1D and S1C). The expression of enterocyte-specific genes *Apob*, *Aqp8* and *Enpep* remained unchanged in *Il17ra*$^{fl/fl}$*;Villin-cre* mice (Figure S1D). Furthermore, we did not detect a difference in the expression of the Paneth cell marker *Lyz1* in the ileum of 6-week-old *Il17ra*$^{fl/fl}$*;Villin-cre*$^{+}$ and *Il17ra*$^{-/-}$ mice (Figures 1D and S1C). We previously observed that *Il17ra*$^{fl/fl}$*;Villin-cre*$^{+}$ mice have increased IL-22 mRNA in the ileum (Kumar et al., 2016), which was also confirmed in 6-week-old *Il17ra*$^{-/-}$ mice (Figure S1E). *Lyz1* expression is a component of an antimicrobial program that is induced by IL-22 (Gaudino et al., 2020; Zha et al., 2019). Additionally, IL-22 production is developmentally regulated coinciding with the maturation of the microbiota and lymphoid compartments (Mao et al., 2018). We also confirmed the induction of *Lyz1* when we treated the organoids from *Il17ra*$^{fl/fl}$*;Villin-cre* mice with recombinant IL-22 (Figure 1E). Therefore, the differences in IL-22 among mouse strains at earlier time points may mask a potential direct role of IL-17A on *Lyz1* expression. To test this, we analyzed the terminal ileum at 10 weeks of age when there is no difference in *Il22* expression (Figure S1F) and found that *Lyz1* expression was reduced in *Il17ra*$^{fl/fl}$*;Villin-cre*$^{+}$ mice compared to cre^{-} mice (Figure 1F). Consistent with our transcript data, the numbers of alcian blue stained cells (indicative of both Paneth and goblet cells) and LYZ1^{+} cells were reduced in the terminal ileum of *Il17ra*$^{fl/fl}$*;Villin-cre*$^{+}$ mice (Figures 1G and 1H).

IL-17A is produced by multiple lymphoid cell types. IL17RA-deficiency could alter the source of IL-17A. However, we found that the frequency of IL-17A^{+} T and non-T cells in the lamina propria of the small intestines were not altered in *Il17ra*$^{fl/fl}$*;Villin-cre* mice (Figure S1G).

Our organoid data suggest a role for IL-17A, which has a much greater affinity for the IL-17R/C complex than IL-17F. The more distantly related homologs IL-17C and IL-25 may also contribute to the *in vivo* secretory cell differentiation defects because they signal through IL-17RA complexed with IL-17RE and IL-17RB, respectively (McGeachy et al., 2019). However, we did not observe decreased expression of secretory cell markers in *Il17re*$^{-/-}$ and *Il17c*$^{-/-}$ mice (Figure S1H). Given that IL-25 is known to indirectly regulate goblet and tuft cell differentiation through a positive feedback loop during a type 2 immune response (von Moltke et al., 2016), we examined whether direct stimulation of epithelial cells can promote secretory cell differentiation. However, we found that IL-25 was toxic to organoids and lowering the dose did not improve viability, preventing us from measuring markers of differentiation (Figure S1I). Collectively, IL-25 does not broadly induce secretory cell lineage compartments, consistent with observations in naïve *Il25*$^{-/-}$ mice (von Moltke et al., 2016). Thus, we focused on IL-17A.

Next, we analyze the effect of intestinal epithelial-specific inhibition of MyD88, an adaptor downstream of the IL-1 receptor and several toll-like receptors (TLRs) but not IL-17RA. MyD88 and IL-17RA both signal via TRAF6 and NF-κB, and MyD88 mediates sensing of intestinal bacteria by Paneth cells and other epithelial lineages (Frantz et al., 2012; Vaishnava et al., 2008). However, *MyD88*$^{fl/fl}$*;Villin-cre*$^{+}$ and cre^{-} mice displayed similar expression of *Dclk1*, *Chga*, *Clca1*, *Muc2* and *Lyz1* (Figure S1J). Therefore, inhibition of major signaling pathways shared by IL-17RA does not necessarily promote secretory cell defects under homeostatic conditions. Collectively, our data suggest that specific IL-17A signaling in the intestinal epithelial compartment supports secretory cell lineage commitment.

IL-17RA promotes intestinal secretory cell differentiation post-development through ATOH1

Secretory epithelial cell defects in *Il17ra*$^{fl/fl}$*;Villin-cre*$^{+}$ mice could reflect events that occur during early development or be due to changes in the microbiota. To circumvent these issues, we generated tamoxifen-inducible knockout *Il17ra*$^{fl/fl}$*;Villin-cre*^{ERT2} mice. We confirmed that the injection of tamoxifen to 8-week-old *Il17ra*$^{fl/fl}$*;Villin-cre*^{ERT2} mice led to reduced expression of *Il17ra* (Figure 2A). With the exception of the tuft cell marker *Dclk1*, we found reduced expression of secretory cell-specific genes in the terminal ileum of *Il17ra*$^{fl/fl}$*;Villin-cre*$^{ERT2+}$ mice compared to cre^{-} controls (Figure 2B). Except for *Apob*, the expression of enterocyte-specific genes (*Aqp8* and *Enpep*) remained unchanged in both groups (Figure 2B). The expression of *Il17ra* positively correlated with secretory markers including *Dclk1*, *Chga* and *Clca1* (Figure S2A). Furthermore, *Il17ra*$^{fl/fl}$*;Villin-cre*^{ERT2} mice displayed reductions in ATOH1^{+} and LYZ1^{+} cells in the ileum (Figures S2B and S2C). These results indicate that IL-17RA signaling regulates secretory epithelial differentiation under homeostatic conditions.

Given the dependence of secretory cell differentiation on the transcription factor ATOH1 (Durand et al., 2012; Yang et al., 2001), we postulated that defects in *Il17ra* deficient mice reflected a role for IL-17A in regulating ATOH1. Indeed, we found reduced *Atoh1* expression in the terminal ileum of naïve *Il17ra*$^{-/-}$ and *Il17ra*$^{fl/fl}$*;Villin-cre*$^{+}$ mice (Figures

2C and 2D). In line with these observations, IL-17A stimulation led to the induction of EGFP$^+$ cells in organoids derived from ATOH1-EGFP transgenic mice (Figure 2E). To confirm that the expression of secretory cell markers post-development is ATOH1-dependent, we analyzed *Atoh1-cre*$^{ER\text{-}T2/flox}$*;Rosa*^{Tdtomato} mice which do not express *Atoh1* upon treatment with tamoxifen (see methods). As expected, tamoxifen administration led to an almost 100% loss of goblet, Paneth and enteroendocrine cell-specific transcripts and alcian blue-stained cells in cre$^+$ mice (Figures 2F and S2D). Furthermore, we observed an approximately 50% reduction in tuft cells based on *Dclk1* expression and immunofluorescence microscopy (Figures 2F–2H), suggesting the potential existence of ATOH1-dependent and independent tuft cell subsets. This potentially explains the inconclusive effect of inducible *Il17ra* deletion on *Dclk1* (Figure 2B). Together, these results indicate that IL-17RA regulates ATOH1-dependent differentiation of secretory epithelial cells post development.

IL-17A regulates the Lgr5$^+$ ISC niche and Paneth cell differentiation via ATOH1$^+$ cells after injury

IL-17A-dependent regulation of secretory cell lineages may be mediated by IL-17RA signaling in Lgr5$^+$ ISCs and/or ATOH1$^+$ progenitor or secretory cells. Analysis of our single cell RNA-seq of mouse small intestinal organoids (GSE159423) confirmed that *Il17ra* and *Il17rc* but not *Il17rb*, *Il17rd* and *Il17re* (not detected), the receptors for IL-17, are expressed on multiple cell types including ISCs and secretory progenitor cells (Figures 3A and S2E). We further confirmed that *Il17ra* and *I17rc* are highly expressed in fully differentiated small intestinal organoids (Figure 3B). To validate this observation in tissues, we sorted double positive RFP$^+$EGFP$^+$ (Lgr5$^+$ ISCs) and RFP$^+$EGFP$^-$ (differentiated epithelial) cells from the ileum of *Lgr5-EGFP-cre*^{ERT2}*;ROSA-CAG-LSL-tdTomato* lineage tracer mice treated with tamoxifen as described (Sato et al., 2011b). We also sorted EGFP$^+$ cells corresponding to secretory progenitor cells and mature secretory epithelial cells from the ileum of *Atoh1-EGFP* transgenic mice. RT-PCR analysis of sorted cells indicated that *Il17ra* and *Il17rc* were expressed by Lgr5$^+$ ISCs and ATOH1$^+$ cells (Figures S2F and S2G). The expression of *Il17rb*, *Il17rd* and *Il17re* in Lgr5$^+$ ISCs (EGFP$^+$RFP$^+$) and differentiated epithelial cells (EGFP$^-$RFP$^+$) were minimal (Figure S2F).

We next generated *Il17ra*$^{fl/fl}$*;Atoh1-cre* mice to examine the role of IL-17RA signaling in ATOH1$^+$ cells (Figure S3A). We confirmed IL-17A production by CD45$^+$ leukocytes was not disrupted in the small intestine lamina propria of *Il17ra*$^{fl/fl}$*;Atoh1-cre* mice (Figure S3B). In contrast to *Il17ra*$^{fl/fl}$*;Villin-cre*$^+$ mice, we found no difference in the expression of *Dclk1*, *Chga*, *Muc2* and *Lyz1* as well as alcian blue-stained and LYZ1$^+$ cells in the terminal ileum and distal colon of *Il17ra*$^{fl/fl}$*;Atoh1-cre*$^+$ and cre$^-$ mice (Figures 3C and S3C–S3E). Given the importance of ATOH1 in regulating Lgr5$^+$ ISC self-renewal after injury (Castillo-Azofeifa et al., 2019; Tomic et al., 2018), we hypothesized that the role of IL-17A signaling in ATOH1$^+$ cells would be evident following administration of dextran sodium sulfate (DSS) in the drinking water, a model of chemical injury and intestinal inflammation. *Il17ra*$^{fl/fl}$*;Atoh1-cre*$^+$ mice displayed exacerbated weight loss, colon length shortening, reduced goblet cell number and tissue damage in the distal colon compared to littermate cre$^-$ mice following DSS treatment (Figures 3D–3F and S3F). Of note, goblet

cell numbers were not reduced in naïve *Il17ra*$^{fl/fl}$*;Atoh1-cre* mice in the absence of DSS (Figure S3F). Although its primary effects are observed in the colon, DSS treatment has subtle effects on the ileum by reducing the number of Paneth cells (Cadwell et al., 2010; Matsuzawa-Ishimoto et al., 2017; Schmitt et al., 2018). We confirmed that the inflammatory marker *Lcn2* was increased in the ileum of DSS-treated *Il17ra*$^{fl/fl}$*;Atoh1-cre* mice (Figure S3G). Also, we found reduced expression of *Lyz1* and a trend towards decreased *Muc2* expression in the terminal ileum of *Il17ra*$^{fl/fl}$*;Atoh1-cre*$^{+}$ mice on day 9 of DSS treatment (Figure 3G). We did not see a difference in *Dclk1* and *Chga* transcripts (Figure 3G). The reduction of *Lyz1* expression corresponded with reduced immunofluorescence staining of ileal tissues (Figure 3H). However, expression patterns of cytokines (*Tnfa Il17a*, *Il6, Il1b* and *Ifng*) were unaltered in the terminal ileum of *Il17ra*$^{fl/fl}$*;Atoh1-cre*$^{+}$ and cre^{-} mice on day 9 of DSS treatment, indicating that these results are not due to overt enteritis, consistent with this preferential impact of DSS on the colon (Figure S3H). Collectively, our data suggest that IL-17RA signaling via ATOH1 regulates colitis susceptibility and possibly Paneth cell differentiation during injury.

Paneth cell-specific IL-17RA signaling is dispensable for DSS-induced colitis and secretory cell differentiation.

Paneth cells, which are enriched in the ileum, have a central role in preventing intestinal inflammation (Adolph et al., 2013) and defects in Paneth cells are a hallmark of Crohn's disease (Cadwell et al., 2008; Gunther et al., 2011; Liu et al., 2016; VanDussen et al., 2014). Since *Atoh1* is also expressed by fully differentiated mature Paneth cells (Lo et al., 2017), it is possible that IL-17RA signaling in Paneth cells regulates their numbers and susceptibility to injury. Therefore, we generated and validated *Il17ra*$^{fl/fl}$*;Defa6-cre*$^{+}$ and cre^{-} mice (Figure 4A). We found no difference in the expression of *Lyz1* transcripts in *Il17ra*$^{fl/fl}$*;Defa6-cre*$^{+}$ and littermate cre^{-} mice under homeostatic conditions (Figure 4B). Next, *Il17ra*$^{fl/fl}$*;Defa6-cre*$^{+}$ and cre^{-} mice were subjected to DSS-mediated intestinal inflammation. Our data indicate no difference in weight loss, colon length shortening and tissue damage in *Il17ra*$^{fl/fl}$*;Defa6-cre*$^{+}$ mice (Figures 4C–4E). We found no difference in the expression of secretory cell-specific transcripts on day 9 of DSS treatment between *Il17ra*$^{fl/fl}$*;Defa6-cre*$^{+}$ and cre^{-} mice (Figure 4F). Overall, these results show that Paneth cell-specific IL-17RA signaling is dispensable for Paneth cell lineage commitment and provides protection against DSS.

Dysregulated *Lgr5* and *Sox9* expression occur in *Il17ra*$^{fl/fl}$*;Atoh1-cre*$^{+}$ mice after DSS-mediated injury

We previously showed that IL-17RA in ATOH1^{+} cells protected mice from colitis and Paneth cell defects following intestinal injury (Figures 3D–3H). However, the mechanism remains unclear. Of note, ATOH1^{+} cells have been shown to regenerate the gut epithelium following injury and replenish depleted numbers of Lgr5^{+} ISCs (Castillo-Azofeifa et al., 2019; Tomic et al., 2018). Additionally, SOX9 regulates epithelial cell proliferation and Paneth cell differentiation (Bastide et al., 2007). Therefore, we examined *Lgr5* and *Sox9* expression in *Il17ra*$^{fl/fl}$*;Atoh1-cre* mice. We found reduced *Lgr5* and *Sox9* expression in the terminal ileum of *Il17ra*$^{fl/fl}$*;Atoh1-cre*$^{+}$ mice on day 9 of DSS treatment but not under

homeostatic conditions (Figures 5A and S4A). Reduced *Sox9* and a trend towards decreased *Lgr5* expression were also evident in the colon of *Il17ra*$^{fl/fl}$*;Atoh1-cre*$^{+}$ mice (Figure 5B).

Our previous analysis focused on the regenerative phase of epithelial injury (day 9, one day after DSS withdrawal). It remains possible that the loss of Paneth cells in *Il17ra*$^{fl/fl}$*;Atoh1-cre*$^{+}$ mice occurs earlier as a direct response to intestinal injury rather than a failure to recover. Therefore, we euthanized *Il17ra*$^{fl/fl}$*;Atoh1-cre*$^{+}$ and cre^{-} mice on day 6 of DSS treatment during the acute injury phase prior to weight loss and reduction in colon length (Figure S4B). However, we found no difference in goblet cells (alcian blue^{+}) and Paneth cells (LYZ1^{+}) in the ileum of *Il17ra*$^{fl/fl}$*;Atoh1-cre*$^{+}$ mice (Figures S4C and S4D). The percentage of IL-17A^{+} T cells and non-T cells also remained unaltered in the lamina propria of *Il17ra*$^{fl/fl}$*;Atoh1-cre*$^{+}$ mice (Figure S4E). In *Il17ra*$^{fl/fl}$*;Atoh1-cre*$^{+}$ mice, IL-17RA signaling remains intact in Lgr5^{+} ISCs. Thus, at this time point, it is possible that IL-17RA signaling in Lgr5^{+} ISCs compensates for the loss of IL-17RA signaling in ATOH1^{+} cells. As expected, our RNA-seq data show increased expression of ISC-related genes (*Lgr5, Sox9, Ascl2*) in the ileum of *Il17ra*$^{fl/fl}$*;Atoh1-cre*$^{+}$ mice (Figure S4F). In line with these observations, the expression of defensins and endoplasmic reticulum stress genes (*Atf4 and Ddit3*) were reduced in the ileum of *Il17ra*$^{fl/fl}$*;Atoh1-cre*$^{+}$ mice (Figure S4F). Furthermore, we observed reduced Ki-67^{+} cells in the colon of *Il17ra*$^{fl/fl}$*;Atoh1-cre*$^{+}$ mice on day 9 of DSS treatment but not in naïve *Il17ra*$^{fl/fl}$*;Atoh1-cre*$^{+}$ mice (Figures S4G–S4I). Of note, there was no difference in the expression of *Mki67, Cdk1* and the number of Ki-67^{+} cells in the ileum of *Il17ra*$^{fl/fl}$*;Atoh1-cre*$^{+}$ mice (Figures S4F and S4J). Collectively, these results show that IL-17RA signaling in ATOH1^{+} cells and possibly Lgr5^{+} ISCs regulates colitis susceptibility and Paneth cell regeneration after injury.

IL-17A signaling in Lgr5^{+} ISCs regulates NF-κB-mediated ATOH1 activity

We observed Paneth cell defects upon intestinal injury in *Il17ra*$^{fl/fl}$*;Atoh1-cre*$^{+}$ mice (Figures 3G and 3H). However, *Il17ra*$^{-/-}$ *Il17ra*$^{fl/fl}$*;Villin-cre*$^{+}$ and tamoxifen-treated *Il17ra*$^{fl/fl}$*;Villin-cre*$^{ERT2+}$ mice displayed pan-secretory cell defects including a reduction in Paneth cells in the absence of injury. Since the defects in Paneth cells were not induced by IL-17RA signaling in mature Paneth cells, we hypothesized that IL-17RA signaling in Lgr5^{+} cells promotes secretory (ATOH1^{+}) cell lineage commitment at steady state. To address this possibility, we sorted EGFP^{hi} (Lgr5^{+} ISCs) cells from *Lgr5-EGFP-cre*$^{ERT2+}$ mice and stimulated them with IL-17A for 24 hours. We found that IL-17A induced *Atoh1* but not *Hes1* in Lgr5^{+} cells (Figures 5C and 5D). Furthermore, we observed that recombinant IL-17A induced the expression of *Atoh1, Lrig1* (stem cell marker) and *Dll1* (progenitor cell marker) in organoids derived from control *Il17ra*$^{fl/fl}$*;Villin-cre*$^{-}$ mice but not IL-17RA-deficient *Il17ra*$^{fl/fl}$*;Villin-cre*$^{+}$ mice (Figure 5E). These results are consistent with the organoid experiments suggesting that IL-17RA signaling promotes secretory cell lineage commitment but not maturation.

Next, we further investigated how IL-17A regulates *Atoh1*. IL-17A has been shown to regulate gene expression by stabilizing mRNA and inducing NF-κB pathways (Amatya et al., 2017). To distinguish between these two possibilities, we cultured organoids in the presence of CHIR99021 (treated for first 2 days) to enrich secretory lineages. When

Atoh1 was measured by RT-PCR in organoids treated with actinomycin D, a transcription inhibitor, the addition of IL-17A did not affect *Atoh1* transcripts (Figure 5F). These results suggest that IL-17A is not capable of stabilizing *Atoh1* mRNA. Therefore, we investigated the possibility that IL-17A regulated *Atoh1* expression through NF-κB. The analysis of both mouse and human *Atoh1* promoters identified several NF-κB binding motifs upstream (~2300bp) of the transcription start site (Figures 5G and S5A). We further performed flow cytometry to evaluate NF-κB activation in IL-17A stimulated Lgr5^{+} ISCs. We used small intestinal organoids from *Il17ra*$^{fl/fl}$*;Lgr5-EGFP-cre*^{ERT2} mice without tamoxifen administration to investigate the expression of IκBα in EGFP^{hi} cells (Lgr5^{+} ISCs) (Figure S5B). Our data showed reduced MFI of IκBα in EGFP^{hi} cells after IL-17A treatment (Figure 5H). Finally, IL-17A lost its capacity to induce *Atoh1* expression in organoids cultured in the presence of the NF-κB inhibitor piceatannol (PCN) (Figure 5I). Collectively, we demonstrate that IL-17A acts on Lgr5^{+} ISCs to initiate an ATOH1-dependent secretory cell differentiation program via the NF-κB pathway.

IL-17A regulates ATOH1 activity and secretory cell lineage commitment via Lgr5^{+} ISCs

To further investigate the regulation of ATOH1 by IL-17A in Lgr5^{+} ISCs *in vivo*, we generated tamoxifen inducible Lgr5^{+} ISC-specific *Il17ra*$^{fl/fl}$*;Lgr5-EGFP-cre*^{ERT2} mice to examine the effects of inducible *Il17ra* deletion. We sorted EGFP^{hi} cells from the small intestine 5 days after the last tamoxifen or corn oil injection (Figure 6A) and confirmed the knockout of *Il17ra* (Figure S5C). RT-PCR data revealed reduced expression of *Atoh1* in tamoxifen-administered sorted EGFP^{hi} cells, again supporting the idea that IL-17RA signaling promotes secretory cell lineage commitment but not maturation (Figure 6B).

Next, we analyzed the expression of *Atoh1* and secretory cell-specific genes in the terminal ileum of tamoxifen administered naïve *Il17ra*$^{fl/fl}$*;Lgr5-EGFP-cre*^{ERT2} mice. Consistent with germ-line *Il17ra*$^{-/-}$ and *Il17ra*$^{fl/fl}$*;Villin-cre*$^{+}$ mice results, we observed reduced expression of *Atoh1, Dclk1, Chga* and *Clca1* expression in *Il17ra*$^{fl/fl}$*;Lgr5-EGFP-cre*$^{ERT2+}$ mice compared to littermate cre^{-} mice (Figures 6C and 6D). However, *Lyz1* expression and LYZ1^{+} cell number were comparable between both groups (Figures 6D–6F) which likely reflects the technical limitations of using *Il17ra*$^{fl/fl}$*;Lgr5-EGFP-cre*$^{ERT2+}$ mice. The half-life of Paneth cells (~30 days) is much greater than other secretory cells (2–3 days) and may not be impacted at 5 days post tamoxifen injection, the time point we analyzed. Therefore, we analyzed the expression of secretory cell-specific genes in the terminal ileum of naïve *Il17ra*$^{fl/fl}$*;Lgr5-EGFP-cre*$^{ERT2+}$ mice 3 months after the final tamoxifen injection. Although we confirmed the lack of *Il17ra* and *Atoh1* expression in the terminal ileum of *Il17ra*$^{fl/fl}$*;Lgr5-EGFP-cre*$^{ERT2+}$ mice (Figures 6G and S5D), we did not find a reduction in the expression of *Lyz1* and LYZ1^{+} cells in the terminal ileum 3 months after the last tamoxifen injection in *Il17ra*$^{fl/fl}$*;Lgr5-EGFP-cre*$^{ERT2+}$ mice when compared to control mice (Figures 6G and 6H). From this we conclude that inducible deletion of IL-17RA leads to general defects in secretory cell differentiation, but compensatory mechanisms may be present that mask the decrease in LYZ1^{+} Paneth cells, such as IL-22 responses or incomplete receptor deletion in Paneth cells.

Consistently, we observed increased *Il22* expression in the ileum of *Il17ra*$^{fl/fl}$*;Lgr5-EGFP-cre*$^{ERT2+}$ mice (Figure 6I) despite the variability among different litters. This observation was reminiscent of our earlier results in *Il17ra*$^{-/-}$ and *Il17ra*$^{fl/fl}$*;Villin-cre*$^{+}$ mice, where elevated *Il22* responses appeared to compensate for the lack of IL-17RA signaling by inducing *Lyz1* expression. We also showed that IL-22 was capable of inducing *Lyz1* expression (Figure 1E). To determine whether excess IL-17A can compensate for IL-22 deficiency, we examined *Rorc*$^{-/-}$ mice, which lack both IL-17A− and IL-22-producing cells. We previously showed that *Rorc*$^{-/-}$ mice have a reduced number of MMP7^{+} Paneth cells as well as expression of *Lyz1* (Gaudino et al., 2020) which we reproduced (Figure S5E). Administration of an adenovirus expressing IL-17A (but not empty vector) to *Rorc*$^{-/-}$ mice led to an increased number of LYZ1^{+} cells in the terminal ileum (Figure S5F). Thus, IL-17A and IL-22 signaling can both affect *Lyz1* expression of Paneth cells and can compensate for one another.

In summary, IL-17A induces *Atoh1* expression in Lgr5^{+} ISCs and inducible deletion of IL-17R inhibits secretory cell differentiation. In contrast, deleting IL-17R in ATOH1^{+} cells compromises the intestinal injury response but does not lead to defects in secretory cell differentiation at steady state. Collectively, these findings support a role for IL-17A in regulating secretory cell lineage commitment and mucosal host defense via the Lgr5^{+} ISC-ATOH1 axis.

IL-17A rescues secretory cell lineage defects in human intestinal organoids

Finally, we turned to human intestinal organoids to determine whether the role of IL-17A in promoting differentiation of secretory epithelial cells is conserved. In contrast to organoids derived from inbred genetically identical mice, we and others have observed heterogeneity in the growth, morphology, and viability of organoids derived from pinch biopsies obtained during endoscopy of human donors (Borten et al., 2018; Fujii and Sato, 2020; Matsuzawa-Ishimoto et al., 2020). While expanding human small intestinal organoids using conventional culturing methods, we noted that a subset spontaneously formed buds, a marker of increased differentiation, while others remained cystic (Figure 7A). However, it is unclear whether these differences reflect an intrinsic property of the epithelial stem cell and donor. For instance, the exact site and depth of the biopsies could affect the cell type composition of the initial culture, leading to inter-individual differences that persist. Such differences could potentially interfere with our ability to investigate IL-17A function.

To overcome this issue, we analyzed the effect of adding recombinant human IL-17A (rhIL-17A) to single cell-derived organoids generated by modifying a previous technique for developing a 2D human intestinal monolayer (Thorne et al., 2018). We applied this technique to examine four persistently cystic organoids and five budding organoids, which we designated as responsive (R1–4) and unresponsive (UR1–5) based on results obtained below. We confirmed that *IL17RA* and *IL17RC* expression are readily detected. Unlike the mouse organoids, we also detected the expression of other IL-17 receptor family members *(IL17RB*, *IL17RD*, and *IL17RE*) (Figure S6A). IL-17 receptor genes generally displayed similar expression when comparing organoid lines with and without rhIL-17A treatment, although we observed a non-statistically significant trend indicating that the *IL-17RA*

mRNA expression may be modestly higher in R1–4 compared with UR1–5 (Figures S6B and S6C). Untreated single cell-derived organoids retained the bud-forming propensity of the original expanded organoid – R1–4 were persistently cystic and UR1–5 displayed spontaneous budding (Figures 7A and 7B).

Although we noted variability in efficiency of organoid formation on day 0, the percentage of organoids per input cell did not correlate with morphology or rhIL-17A treatment (Figure 7C). We also did not find any relationship between morphology and age, sex, or disease status of the donor (Table S1). Cystic organoids (R1–4) cultured in the presence of rhIL-17A responded by generating buds as early as day 4 while mock treated controls remained bud-free (Figure 7B). In contrast, the morphology of organoids that display spontaneous budding (UR1–5) was not further affected by rhIL-17A treatment (Figure 7B). All organoids exhibited comparable viability and cell death, which was not affected by the presence of rhIL-17A, even after prolonged culture (day 10) (Figures 7D and 7E). Thus, stably cystic organoid subsets respond to rhIL-17A by forming buds.

Our findings in mice indicate that IL-17A promotes differentiation towards secretory lineages through inducing *Atoh1* expression. Similarly, rhIL-17A induced a 4–10-fold increase in *ATOH1* expression in R1–4 organoids but not in UR1–5 (Figures 7F and S6D). Instead, UR1–5 showed 15–20-fold higher expression of *ATOH1* compared with R1–4 in the absence of rhIL-17A (Figure S6E). Treatment with rhIL-17A also led to a general increase in the expression of the secretory epithelial genes *MUC2*, *CLCA1*, and *CHGA* in R1–4 organoids, similar to murine organoids (Figure 7F). The increase in these secretory cell markers correlated well with *ATOH1* expression and did not occur in UR1–5 (Figures 7G and S6D). Furthermore, rhIL-17A treatment did not affect expression of the stem cell marker gene *LGR5*, the Notch signaling receptor gene *NOTCH1*, the ATOH1 repressor-encoding gene *HES1*, and the canonical Wnt suppressor gene *AXIN2* in either type of organoids (Figure S6F). Also, in contrast to secretory markers, the expression of enterocyte markers either decreased (*APOB*) or remained the same (*FABP2*, *ENPEP*, and *AQP8*) in both R1–4 and UR1–5 following rhIL-17A treatment, suggesting that the ability of IL-17A to enhance epithelial differentiation is specific to secretory cells (Figure S6F).

Consistent with the transcript analysis, immunofluorescence microscopy analysis showed that rhIL-17A increased ATOH1$^+$ cells in R1–4 organoids without changing the total number of cells per field (Figures 7H, 7J, S7A, and S7D). This increase in ATOH1$^+$ cells was observed at the individual organoid (Figure S7B). Additionally, the increase in ATOH1$^+$ cells induced by rhIL-17A was accompanied by a similar increase in MUC2$^+$ and CHGA$^+$ cells, especially in R3 and R4 (Figures 7I, 7K, S7C, and S7E). All together, these results indicate that human intestinal organoids display stable differences in their propensity to spontaneously differentiate and respond to IL-17A. Organoids with an immature cystic morphology display a conserved response to the presence of IL-17A that entails an increase in secretory cell differentiation.

Discussion

IL-17A has been shown to regulate the gut epithelial barrier, IgA transcytosis and gut microbiota colonization via the IL-17RA-IL-17RC receptor complex (Kumar et al., 2016; Maxwell et al., 2015). Despite this appreciation that IL-17A contributes to the mucosal immune environment of the gut, it was unknown whether and how IL-17A interacts with functionally distinct intestinal cell types. Our findings revealed a conserved function of IL-17A in epithelial cell lineage commitment. Our results from germ-line intestinal epithelial cell-specific *Il17ra* knockout mice (*Il17ra*$^{fl/fl}$*;Villin-cre*) revealed a reduction in secretory cell-specific genes and the number of LYZ1^{+} and alcian blue^{+} cells. These data were reproduced in tamoxifen inducible *Il17ra*$^{fl/fl}$*;Villin-cre*^{ERT2} mice and IL-17A stimulated primary intestinal organoids. However, we observed that *Lyz1* and *Muc2* did not positively correlate to *Il17ra* expression in *Il17ra*$^{fl/fl}$*;Villin-cre*^{ERT2} mice. The perceived discrepancy may be related to variation in *Il17ra* mRNA expression or differences in the gut microbiota. We noticed that *Il17ra*$^{fl/fl}$*;Villin-cre*$^{ERT2-}$ control mice express varying mRNA of *Il17ra* as shown in Figure 2A. While *Il17ra*$^{fl/fl}$*;Villin-cre*$^{+}$ mice possess germ-line knockout of *Il17ra*, knockout of *Il17ra* in *Il17ra*$^{fl/fl}$*;Villin-cre*$^{ERT2+}$ mice may be more variable since it depends on the efficacy of and response to injection with tamoxifen.

In our murine organoid system, CHIR is present from day 0 to day 2. We reveal that CHIR is required for IL-17RA-mediated induction of *Atoh1* and secretory cell markers. CHIR is a highly selective GSK3 inhibitor. By inhibiting GSK3, CHIR activates Wnt signaling. Wnt signaling has been shown to be important for the self-renewal and function of Lgr5^{+} ISCs (Li et al., 2018; Mah et al., 2016; Yin et al., 2014). Therefore, the initial activation of Wnt signaling in stem cells may be involved in IL-17RA-mediated induction of *Atoh1* and secretory cell lineage commitment. *In vivo*, continuous sources of Wnt are present in the gut epithelium from various cell types such as stromal cells and Paneth cells (Gregorieff et al., 2005; Sato et al., 2011b). Our data indicate that the requirement of CHIR for IL-17RA-mediated secretory cell lineage commitment in organoid systems is representative of normal physiological processes in the gut mucosa.

ATOH1^{+} secretory progenitor cells are required for goblet, Paneth and enteroendocrine cell development (Yang et al., 2001). IL-17RA signaling in ATOH1^{+} cells was dispensable under steady-state conditions, providing additional evidence that IL-17A acts on other cell types such as Lgr5^{+} ISCs rather than ATOH1^{+} secretory progenitor cells. However, *Il17ra*$^{fl/fl}$*;Atoh1-cre*$^{+}$ mice displayed an aberrant intestinal injury response consisting of a reduction of Paneth cells in the ileum and epithelial proliferation in the colon, along with other signs of exacerbated inflammation. Of note, Paneth cells remained intact on day 6 post DSS treatment, while *Il17ra*$^{fl/fl}$*;Defa6-cre*$^{+}$ mice retained a normal injury response, indicating that IL-17RA signaling is dispensable in differentiated Paneth cells. Castillo-Azofeifa et al showed that Lgr5^{+} ISC numbers were reduced following DSS administration and were dispensable to regenerate the colonic epithelium after DSS-induced colitis (Castillo-Azofeifa et al., 2019). Indeed, a lineage tracing study showed that cells derived from ATOH1^{+} precursors greatly expand and regenerate the colonic epithelium as well as replenish Lgr5^{+} ISCs after intestinal injury (Castillo-Azofeifa et al., 2019; Tomic et al., 2018). Thus, it remains possible that IL-17A acts on ISCs derived from

ATOH1^{+} precursors during injury. We found that IL-17RA signaling in ISCs promoted *Atoh1* expression and differentiation of these major secretory cell types. Furthermore, we provide evidence supporting that IL-17A regulates lineage commitment but not secretory cell maturation. We sorted Lgr5^{+} ISCs and showed that IL-17A treatment promotes the expression of *Atoh1* after 24 hours of stimulation. This demonstrates that IL-17A acts on ISCs early during their development to promote their differentiation into secretory cells. We also observed that IL-17A treatment promoted increased expression of *Atoh1* and *Dll1* (marker for precursor cells committed to differentiating into secretory cells) in *Il17ra*$^{fl/fl}$*;Villin-cre* organoids. Moreover, we isolated Lgr5^{+} ISCs from *Il17ra*$^{fl/fl}$*;Lgr5-EGFP-cre*$^{ERT2+}$ mice and confirmed the reduction of *Atoh1* expression in Lgr5^{+} ISCs after knockout of *Il17ra*. In addition, differentiated organoids that already contained secretory cells did not respond to IL-17A with further increases in the expression of secretory cell markers, indicating that the role of IL-17A is unlikely explained through effects on these markers during maturation after lineage commitment. Taken together, our findings indicate that IL-17A promotes secretory cell lineage commitment by Lgr5^{+} ISCs during homeostasis, with a related role in supporting cells derived from ATOH1^{+} cells during recovery from injury.

It is possible that the role of IL-17A in promoting secretory cell development including Paneth cells that we uncovered contributes to the adverse intestinal events associated with IL-17A and IL-17RA blockade. A reduction in Paneth cell numbers and antimicrobial function has been reported in Crohn's disease patients (Liu et al., 2016), especially in individuals harboring a disease-associated variant of *ATG16L1* (Cadwell et al., 2008). In this context, it is notable that IL-17A treatment promotes secretory cell differentiation in human organoids. In contrast, a recent study showed that IL-17A is cytotoxic when added to colonic organoids, providing an explanation as to why mutations in the IL-17 signaling pathway accrue in the epithelium during colitis-associated cancer (Nanki et al., 2020). This previous study used 10-fold excess IL-17A (100 ng/ml compared with 10 ng/ml in our study) to mimic the conditions associated with colorectal cancer that occurs in ulcerative colitis patients. In addition to the concentration of IL-17A, it is also possible that the anatomical regions (small intestine versus colon) or media supplements (e.g., Noggin) contribute to discrepant findings (Middendorp et al., 2014; Sato et al., 2011a). Given the different conditions of the assays, which reflect the goals of the two studies, we do not believe our results contradict the findings from Nanki et al.

In addition to validating our results from mice, our human organoid experiments uncovered differences in morphology between donors, a feature that was stable after single cell plating. Intestinal organoid heterogeneity has mainly been described for those derived from tumors and is linked to the somatic mutational landscape (Fujii and Sato, 2020). Mechanisms contributing to the heterogeneity among 'normal' organoids has remained largely obscure. We recently demonstrated that differential susceptibility to TNFα-induced death of organoids is due to the *ATG16L1* Crohn's disease risk variant (Matsuzawa-Ishimoto et al., 2020). Aberrant TNFα signaling was associated with a spontaneous interferon signature, which we found enhances intestinal epithelial responses that can be either adverse or protective in the presence of different microbial challenges in mice (Marchiando et al., 2013; Martin et al., 2018; Matsuzawa-Ishimoto et al., 2017; Neil et al., 2019). Thus,

investigating the origin of intestinal organoid heterogeneity may provide insight into how individuals can mount different epithelial responses.

In this study, we demonstrated that the addition of IL-17A to the culture media 'corrected' the inability of cystic organoids to form buds and differentiate secretory cells. Organoids that were unresponsive to IL-17A displayed comparatively high mRNA expression of *AOTH1*, suggesting they are already maximally poised to differentiate and cannot be further induced. Although it is unknown whether there is an underlying genetic explanation that leads to this initial difference in propensity to form buds, our results raise the possibility that individuals have differential dependence on IL-17A. An important future direction is to determine whether such differences contribute to disease susceptibility or treatment responses.

Limitations of the study

Given that goblet and Paneth cells regulate a wide range of functions and play critical roles in maintaining intestinal health, compensatory mechanisms such as IL-22 and IL-13 are present *in vivo* to regulate differentiation into these cell types. This is an important factor to consider and is a possible limitation of our mouse models. In contrast, organoids represent a self-contained system with fewer background signals from non-epithelial cells and confounding variables that may additionally influence gene expression. The induction of Atoh1 and secretory markers by IL-17A in both murine and human organoids further supports our *in vivo* findings. While IL-17A is not the only factor involved in lineage specification, our results altogether provide overwhelming evidence that signaling through IL-17RA is one key factor.

STAR METHODS

RESOURCE AVAILABILITY

Lead contact—Further information and requests for resources and reagents should be directed to and will be fulfilled by the Lead Contact, Pawan Kumar (pawan.kumar@stonybrook.edu).

Materials availability—The materials in the current study are available from the Lead Contact with a completed Materials Transfer Agreement.

Data and code availability—The RNA-seq data have been deposited in Gene Expression Omnibus and are publicly available as of the date of publication. This paper analyzes existing, publicly available scRNA-seq data. These accession numbers for the datasets are listed in the key resources table. This paper does not report original codes. Any additional information required to reanalyze the data reported in this work is available from the Lead Contact upon request.

EXPERIMENTAL MODEL AND SUBJECT DETAILS

Mice—C57BL/6J (WT), *Atoh1-cre* (C57BL/6J background), *Atoh1-EGFP* (C57BL/6J background), and *Villin-Cre* (C57BL/6J background) were purchased from The Jackson Laboratory. *Defa6-Cre* mice were obtained from Dr. Richard Blumberg, Brigham

and Women's Hospital, Harvard. Ileum tissues of Tamoxifen-administered *Atoh1-cre*$^{ERT2/flox}$*;Rosa*^{Tdtomato} mice were obtained from Stephen Maricich, University of Pittsburgh. Generation and characterization of *Atoh1-cre*$^{ERT2/flox}$*;Rosa*^{Tdtomato} mice in which the *Atoh1* locus is disrupted by the *cre*^{ERT2} transgene on one chromosome and the other locus is loxP flanked and excised upon tamoxifen treatment were as described (Wright et al., 2015). *Villin-cre*^{ERT2} and *Lgr5-EGFP-cre*^{ERT2}*; ROSA-CAG-LSL-tdTomato* mice were obtained from Dr. Vincent W. Yang, Stony Brook University. Generation and characterization of IL-17-Floxed (*Il17ra*$^{fl/fl}$) mice were performed as described (Kumar et al., 2016). *Il17ra*$^{fl/fl}$ mice were bred with *Villin-cre*, *Lgr5-EGFP-cre*^{ERT2}, *Atoh1-cre,* or *Defa6-cre* mice to generate entire gut epithelium, ISC-specific, secretory progenitor plus epithelium, and Paneth cell-specific IL-17RA knockout mice. *Il17c*$^{-/-}$ and *Il17re*$^{-/-}$ knockout mice terminal ileum tissues were obtained from Dr. Sarah L. Gaffen, University of Pittsburgh. *Rorc*$^{-/-}$ mice were received from Dr. Jay K Kolls, University of Pittsburgh. We used 6, 10 and 12 week-old mice (both genders) for all experiments unless indicated in the figures. All mice were housed in specific pathogen-free conditions at Stony Brook University, Stony Brook, NY. All animal studies were conducted with the approval of University of Pittsburgh and Stony Brook University Institutional Animal Care and Use Committee.

Cell lines—L-WRN, the mouse male cell line, was obtained from Dr. Thaddeus Stappenbeck at Washington University in St. Louis (Miyoshi and Stappenbeck, 2013). The cell line was directly used from Dr. Thaddeus Stappenbeck.

Human intestinal specimens—Pinch biopsies were obtained with consent from adult healthy subjects or IBD patients undergoing surveillance colonoscopy, using 2.8-mm standard biopsy forceps, after protocol review and approval by the New York University School of Medicine Institutional Review Board (Mucosal Immune Profiling in Patients with Inflammatory Bowel Disease; S12–01137). Inflammation status of tissues was confirmed by pathological examination. Subject information for human specimens is shown in Table S1.

METHOD DETAILS

Induction of gene knockouts—To induce the knockout of genes, tamoxifen (1 mg/mouse) or corn oil was administered intraperitoneally from day 0 to day 4. At 5 days, 7 days or 3 months post last tamoxifen injection, tissues were harvested for RT-PCR and immunofluorescence staining.

For *Atoh1-cre*$^{ER-T2/flox}$*;Rosa*^{Tdtomato} mice, tamoxifen was injected at 27, 28 and 29 days after birth. Tissues were harvested at 7 days post last tamoxifen injection.

Animal treatment—For adenovirus treatment, the construction, generation and quality control of the empty vector (Ad-y5) and adenovirus expressing murine IL-17A (Ad-IL-17A) has been described (Schwarzenberger et al., 1998). *Rorc*$^{-/-}$ mice were injected with Ad-IL-17A or Ad-y5 (1×10^9 PFU/mouse) intraperitoneally. The terminal ileum was harvested at 7 days post injection and processed for immunofluorescence.

For DSS treatment, mice were treated with 2.5% DSS in the drinking water from day 0 to day 8. DSS was changed to normal water on day 8. On day 9, tissues were harvested for further analysis.

RT-PCR—Total RNA was extracted from terminal ileum tissues, distal colon tissues, or organoids using Trizol-based isolation or RNeasy Mini Kit (QIAGEN), and cDNA was synthesized using Bio-Rad iScript kits or High-Capacity cDNA Reverse Transcription Kit (ThermoFisher) according to the manufacturer's protocol. RT-PCR was performed by mixing 5 μl of SsoAdvanced™ Universal Probes Supermix (Bio-Rad) or SsoAdvanced™ Universal SYBR Green Supermix (Bio-Rad) or LIGHTCYCLER 480 SYBR GREEN I master (Roche), 4.5 μl of cDNA and 0.5 μl of primers/probes. RT-PCR analysis for mammalian genes was calculated relative to *Hprt, Gapdh or ACTB*.

Histopathology—5 μm paraffin embedded tissue sections were deparaffinized and rehydrated using Xylene and a descending ethanol gradient (100%, 95%, 70%, pure dH_2O).

For alcian blue staining, 3% acetic acid was applied to the slides for 3 minutes. Alcian blue solution (pH 2.5) was added to slides for 10 minutes to stain the cells. 3% acetic acid was applied to the slides for approximately 30 seconds to remove excess Alcian blue staining. Slides were rinsed in running tap water for 5 minutes followed by 2 changes of distilled water. Nuclear Fast Red Solution (Electron Microscopy Sciences) was applied for 5 minutes to stain the cell nucleus. Slides were rinsed with running tap water for 2 minutes, transferred to 2 changes of distilled water, and then dehydrated with an ascending ethanol gradient (70%, 95%, and 100%). Slides were mounted and images were acquired.

For hematoxylin & eosin (H&E) staining, hematoxylin (VWR) was added to slides for 3 minutes and washed in water for approximately 5 minutes. 3% acetic acid was applied to the slides for approximately 1 minute. Slides were rinsed in running tap water for 5 minutes followed by 2 changes of distilled water. 95% ethanol was applied for 1 minute. Tissues were stained with eosin (VWR) for 1 minute. Slides were transferred to 95% and 100% ethanol for 2 minutes each. Slides were mounted and images were acquired.

Cell Isolation—The ileums were harvested and flushed with ice-cold 1× PBS. Tissues were opened longitudinally and peyer's patches were removed. Then tissues were washed 4 additional times with ice-cold PBS and cut into 2-cm pieces.

For lamina propria leukocyte isolation, the tissue pieces were incubated in 30 ml of 1× Hank's Balanced Salt Solution (HBSS, ThermoFisher) containing 1.3 mM of EDTA for 15 min at 37 °C with shaking. Repeat EDTA digestion once. After washing with ice-cold 1×PBS, tissues were transferred to 3 ml of RPMI-1640 (Hyclone) containing 1% FBS (Gibco) and 0.05 mg/ml of liberase TL (Roche). Digested tissues were then filtered through 70 μm strainer and washed with RPMI-1640 containing 1% FBS. Cells were pelleted, resuspended in 2.5 ml of 44% percoll (Cytiva) and added to the top of 67% percoll (2 ml). Cell suspension was centrifuged at 1600×g, 25 °C for 20 min without brake. The leukocytes were harvested, pelleted by centrifuge and processed for flow cytometry. For the crypt isolation, the tissue pieces were incubated in ice-cold 1× PBS containing 3.75 mM

of EDTA on an orbital shaker (60 rpm) for 30 min at 4 °C. Then tissues were washed and crypts were released by shaking tissue pieces in ice-cold 1× PBS. Repeat this step two more times to gather more crypts. The isolated crypts were filtered using a 70-μm cell strainer and processed for organoid culture. Or the isolated crypts were resuspended in DMEM/F12 (Gibco) containing 10% FBS and incubated for 15 min at 4°C. Cells were then dissociated using TrypLE Express (Invitrogen) supplemented with 10 μM Y-27632 (Sigma-Aldrich) and 2.5 μg/ml DNase I (Roche) for 5 min at 37°C. Cells were filtered using a 70-μm cell strainer to remove clumps and mucus. The cells were further washed twice with 1× PBS and pelleted by centrifugation at 4°C at 2000 rpm for 3 min. Cell suspension was processed for fluorescence-activated cell sorting (FACS) of $EGFP^{hi}$ cells at BD FACSAria. Sorted cell were seeded immediately for acute IL-17A stimulation or lysed for RT-PCR.

Culture of Murine and Human Intestinal Organoids—For the culture of murine intestinal organoids, crypts were pelleted and re-suspend in Matrigel Matrix (Corning) at a concentration of 80 crypts per 20 μl Matrigel. 20 μl of crypt suspension were distributed to 24-well plates. After the polymerization of Matrigel at 37°C, 5% CO_2 for 30 min, the matrix was overlaid with 500 μl of Organoid Growth Medium (1:1 mixture of L-WRN and DMEM/F12) containing 1× penicillin-streptomycin-glutamine (Invitrogen), 1× N2 (Invitrogen), 1× B27 (Invitrogen), 50 ng/mL of human (h)EGF (R&D system), 1 mM of N-acetylcysteine (Sigma-Aldrich), 10 nM of Gastrin-Leu15 (Sigma-Aldrich), 500 nM of A83–01 (Torics), 10 μM of Y-27632 (Sigma-Aldrich) and 10 μM of CHIR99021 (Tocris). Organoid Growth Medium was changed every 2 days and CHIR99021 was removed on day 2. 10 μM of Piceatannol (EMD Millipore) was added on day 0 in indicated experiments. Organoids were treated with IL-17A (50 ng/ml) or IL-22 (10 ng/ml) and harvested on day 5 or day 6 for RT-PCR. Images were taken on day 5 or day 6 with an Olympus CKX41 microscope. In Figure 1C, organoids were only treated with IL-17A (50 ng/ml) on day 5 for 7 hours.

Human organoids were cultured as described previously (Matsuzawa-Ishimoto et al., 2020; Neil et al., 2019). Pinch biopsies were collected in ice-cold complete RPMI (RPMI 1640 medium supplemented with 10% fetal bovine serum (FBS), penicillin/streptomycin/glutamine, and 50 μM 2-mercaptoethanol). They were incubated in Gentle Cell Dissociation Reagent (Stemcell Technologies) on ice for 30 min, followed by vigorous pipetting to isolate crypts. The crypts were embedded in 30 μl of Matrigel and cultured with maintenance media (human IntestiCult Organoid Growth Medium, Stemcell Technologies). The culture medium was changed every 2–3 days. For passing human organoids, 10 μM Y-27632 were added for the first 2 days.

On day 5, the organoids were incubated in 500 μl of cell recovery medium (Corning) at 4°C for 30 min to depolymerize the Matrigel. Then the organoid suspension was pelleted at 2000 rpm, 4°C for 5 min and washed with 1× PBS once. After adding 500 μl of TrypLE express (Gibco) containing 0.05 mM of N-acetylcysteine and 10 μM of Y-27632, the resuspended cells were incubated at 37°C for 5 min. Cells were then pelleted after the addition of 500 μl of 1× PBS containing 5% FBS and processed for flow cytometry.

Flow Cytometry—For IL-17A staining, cells were incubated in IMDM (Gibco) containing 10% FBS and Leukocyte Activation Cocktail with BD GolgiPlug (BD) at 5% CO_2, 37 °C

for 4 hours in a round bottom 96-well plate. After incubation, cells were washed with 200 μl of FACS Buffer (1× PBS containing 1% BSA and 0.01% NaN_3) and incubated in 100 μl of FACS Buffer containing aqua fluorescent reactive dye (Invitrogen, 1:500), anti-CD45 (eBioscience, 30-F11, 1:100) and anti-CD3 (eBioscience, 145–2C11 1:100) at 4°C for 30 min. Then cells were washed with FACS Buffer and incubated in 100 μl of IC Fixation Buffer (eBioscience) at 4 °C for 20 min. Following the wash with 1× Permeabilization Buffer (eBioscience), the fixed cells were incubated in 100 μl of 1× Permeabilization Buffer containing anti-IL-17A (eBioscience, eBio1787, 1:100) at 4 °C overnight. The next day, cells were washed with 1× Permeabilization and resuspended in FACS Buffer for further analysis with BD LSR Fortessa flow cytometer.

For IκBα staining, the isolated cells from organoids were washed with 200 μl of FACS Buffer and incubated in 100 μl of FACS Buffer containing aqua fluorescent reactive dye (Invitrogen, 1:500) at 4°C for 30 min. Following the wash with FACS Buffer, the cells were incubated in 100 μl of IC Fixation Buffer at 4 °C for 20 min. Then cells were washed with 1× Permeabilization Buffer and incubated in 100 μl of 1× Permeabilization Buffer containing anti-IκBα (eBioscience, MFRDTRK, 1:100) at 4 °C overnight. The next day, cells were washed with 1× Permeabilization and resuspended in FACS Buffer for further analysis with BD LSR Fortessa flow cytometer.

Single Cell-derived Human Organoids—Mature human organoids grown with the maintenance media were digested into single cells using TrypLE Express and suspended thoroughly in 30 μl Matrigel at 100, 300, or 500 cells/μl, respectively. For differentiation, the maintenance media was replaced with DMEM/F-12 (ThermoFisher) in the presence of 100 IU Penicillin and 100 μg/ml Streptomycin (Corning), 125 μg/ml Gentamicin (ThermoFisher), 2 mM L-Glutamine (Corning), 20 ng/ml mouse (m)EGF (PeproTech), 100 ng/ml mNoggin (R&D systems), 1 μg/ml hR-Spondin 1 (R&D systems), 100 ng/ml mWnt-3a (R&D systems), 1 mM *N*-acetylcysteine (Sigma-Aldrich), 10 nM hGastrin (Sigma-Aldrich), 500 nM A-83–01 (Tocris), 200 ng/ml hIGF-1 (Biolegend), 100 ng/ml hFGF-2 (Peprotech), and 1× B27, herein referred as IF medium (Fujii et al., 2018). Each 10 μl drop was cultured in 96 -well culture plate in triplicates with or without 10 ng/ml rhIL-17A (R&D systems) for the first 3 days. Generation efficiency was determined by quantifying the intact number of organoids on day 0. The organoids were washed 3 times using advanced DMEM/F12 to remove Y-27632 and then cultured in the IF medium treated with ± 10 ng/ml rhIL-17A for another 10 days. The culture medium was changed every 3 days. Percent viable organoids were determined by quantification of the number of intact organoids on days 0 and 10. Opaque organoids with condensed structures or those that have lost adherence were excluded. For thiazolyl blue tetrazolium bromide (MTT) reduction assay, staining with MTT was adapted from a previously described method (Matsuzawa-Ishimoto et al., 2020). In brief, we added MTT (Sigma-Aldrich) into the organoids treated with ± 10 ng/ml rhIL-17A to a final concentration of 500 μg/ml on day 10. After incubation for 2 h at 37°C, 5% CO_2, the medium was discarded and 20 μl of 2% SDS (Sigma-Aldrich) solution in water was added to solubilize the Matrigel for 2 h. Then, 100 μl of DMSO (ThermoFisher) was added for 1 h to solubilize the reduced MTT, and OD was measured on a microplate absorbance reader (ParkinElmer) at 562 nm. The specific organoid death (%)

was calculated as MTT deduction (%) by normalizing to non-stimulated organoids which were defined as 100% viable.

Single Cell RNA Sequencing (scRNA-seq)—scRNA-seq sequences were processed using Cellranger for demultiplexing, UMI (unique molecular identifier) collapsing and alignment to the mm10 mouse transcriptome. In R, raw files were converted into a Seurat object prior to analysis (we utilized Suerat 3.2.1 and ggplot2 3.3.2). Data structures were filtered retaining cells expressing more than 2,500 genes, 10,000 counts, and less than 15% mitochondria counts (1531 cells in the filtered dataset). Data was log-normalized: counts for each cell are divided by the total counts for that cell and multiplied by 10000, and the resulting values are natural log-transformed. Clusters were found via a Louvain clustering algorithm (Seurat) with a resolution of 0.3. Intestinal cells were classified using established metagene lists for the intestinal cell types described in (Ayyaz et al., 2019; Haber et al., 2017). To create a 2D visualization of the cell populations and clusters a UMAP was applied. Log expression of *Il17ra, Il17rb, Il17rc and Il17rd* were projected onto a violin plot and dot plot using Seurat.

RNA Sequencing (RNA-seq)—RNA from the terminal ileum of DSS (day 6) treated *Il17ra*$^{fl/fl}$*;Atoh1-cre*$^{+}$ and their littermate cre^{-} mice was isolated using Trizol extraction methods. To eliminate genomic DNA contamination, isolated total RNA was treated with DNase I and then purified with the RNA Clean & Concentrator −5 Kit (Zymo Research). The library for RNA-Seq analysis was prepared starting from 1 ug RNA. To deplete ribosomal RNA, we used NEBNext rRNA Depletion Kit (NEB) according to manufacturer's protocol. We then prepared strand-specific libraries using the NEBNext Ultra II Directional RNA Library Prep Kit (NEB) according to manufacturer's supplied protocol. Library quality was confirmed by size analysis using Bioanalyzer High Sensitivity DNA Analysis (Agilent). All the libraries were sequenced on an Illimuna NextSeq 500 using high-output kit.

Sequencing analysis was done using RNA-seq for Eukaryotes Analysis v3 by Banana Slug Genomics Center at University of California Santa Cruz. Raw sequencing reads (paired-end reads) that were produced by Illumina sequencer were quality checked for potential sequencing issues and contaminants using FastQC. Adapter sequences and primers were trimmed from the sequencing reads using Trimmomatic, then followed by removing polyA tail, polyN, and read portions with quality score below 28 using PRINSEQ. Reads with a remaining length of fewer than 20 bp after trimming were discarded. A second round of quality check with FastQC was made to compare read quality before and after trimming. Trimmed reads were mapped to the reference genome (GRCm38/mm10) using (TopHat2) with NCBI RefSeq annotated genes as transcriptome index data. Read alignment coverage and summary statistics for visualization were computed using SAMtools, BEDtools, and UCSC Genome Browser utilities. Cufflinks 2.2.0 workflow and read-counting methodology with DESeq and edgeR were adopted for abundance estimation and differential expression analysis. In brief, using Cufflinks workflow, the sequencing reads aligned to RefSeq annotated genes were quantified using Cuffquant. Cuffnorm was then used to normalize the gene expression across the studied samples with FPKM computed for sample correlation assessment. Differential expression analysis between samples was performed using Cuffidff

with the computed results from Cuffquant. Using read-counting methodology, HTSeq was adopted to compute raw read counts for annotated RefSeq genes. Raw read counts were normalized across all samples and then used for differential expression analysis using edgeR.

Immunofluorescence—The terminal ileum was fixed in 10% formalin and embedded in paraffin blocks. Paraffin embedded tissue sections (5 μm) were deparaffinized using xylene and rehydrated using a descending ethanol gradient (100%, 95%, 70%, pure dH_2O). Antigen retrieval was conducted by heating slides in a microwave. Tissues were permeabilized with 1× PBS containing 0.1% Triton X-100 (Sigma-Aldrich) for 10 min at room temperature and washed three times with 1X PBS containing 0.01% Tween 20 (VWR). Then tissue sections were blocked in 1× PBS containing 5% bovine serum albumin for 1 hour at 37°C followed by incubation at 4°C overnight in 1× PBS containing 5% bovine serum albumin and primary antibodies against LYZ1-FITC (1:200), ATOH1 (1:400), and DCLK1 (1:200). After washing the slides with 1× PBS, the sections were incubated with anti-rabbit IgG Fab2 Alexa Fluor® 647 (Cell Signaling Technology, 1:300) or anti-rabbit IgG Fab2 Alexa Fluor® 488 (Cell Signaling Technology, 1:300). Slides were mounted with a DAPI hard stain (Vector® Laboratories, H-1500) to visualize cell nuclei. Images were acquired using a Zeiss 510 Meta NLO confocal microscope (Stony Brook University) or Olympus CKX41 microscope.

For murine organoids, small intestinal organoids were cultured and fixed for 30 min with 4% paraformaldehyde (Electron Microscopy Sciences). Organoids were washed with 1× PBS containing 2.5% bovine serum albumin and 0.01% Tween 20 for 10 minutes. Then organoids were treated for 10 min with 1× PBS containing 2.5% bovine serum albumin and 0.01% Triton X-100 and incubated overnight in primary antibodies against LYZ1-FITC (1:200), UEA1 (1:200), and ATOH1 (1:400). Organoids were washed 3 times and incubated with anti-rabbit IgG Fab2 Alexa Fluor® 488 (Cell Signaling Technology, 1:300). Slides were mounted with a DAPI hard stain (Vector® Laboratories, H-1500) and images were acquired using a Zeiss 510 Meta NLO confocal microscope (Stony Brook University) or Olympus CKX41 microscope.

For human intestinal organoids, frozen sections were prepared by fixing with 4% paraformaldehyde (Electron Microscopy Sciences) and cryprotecting with 20% sucrose (Sigma-Aldrich). Fixed organoids were mixed with NEG-50 (Epredia) and frozen in cryomold with 2-methylbutane (Sigma-Aldrich) cooled by dry ice. 10-μm sections were made by Cryostat (Micron HM350; ThermoFisher). The air-dried sections were permeabilized using 0.2% Triton X-100 (Sigma-Aldrich) solution and incubated with primary and secondary antibodies in 4% (w/v) bovine serum albumin (ThermoFisher)/ phosphate-buffered saline (PBS) (Corning) blocking solution. The following primary antibodies were used: anti-ATOH1 (rabbit, 1:500, Proteintech, 212151AP), anti-MUC2 (rabbit, 1:500, Santa Cruz, SC-15334), anti-CHGA (mouse, 1:100, Santa Cruz, SC-393941). Alexa Fluor 555 conjugated with anti-mouse IgG and Alexa Fluor 488 conjugated anti-rabbit IgG were purchased from ThermoFisher (A28180 and A11008, respectively) and used as secondary antibodies at a final concentration of 1:500. Nuclei were visualized using ProLong™ Glass Antifade Mountant with NucBlue™ Stain (ThermoFisher, P36918).

Images were acquired using an EVOS FL Auto Cell Imaging System (ThermoFisher) and then processed and quantified using ImageJ.

mRNA stability assay—Organoids were incubated either in the absence or presence of recombinant IL-17A (R&D system, 50 ng/ml). After 4 hours, actinomycin D (Sigma-Aldrich, 5 μg/ml) was added to their respective wells. Organoids were harvested in RLT buffer at 0, 1, or 6 hours post the addition of actinomycin D and processed for RT-PCR.

Supplementary Material

Refer to Web version on PubMed Central for supplementary material.

ACKNOWLEDGEMENT

We would like to acknowledge the Flow Cytometry Core at Stony Brook University. We would like to acknowledge the Research Histology Core Laboratory at Stony Brook University. We would like to acknowledge the RNA sequencing core at Cold Spring Harbor Laboratory. We would like to acknowledge the New York University Langone Health (NYULH) Microscopy Lab supported by the National Cancer Institute grant P30 CA016087. We thank Makheni Jean-Pierre and Suzanne Tawch for their help. This work was supported by the Crohn's and Colitis Foundation (476637), DK121798, AI149257 and the SUNY Research Foundation to PK, DE022550 to SLG, DK103788, AI121244, HL123340, DK093668, AI130945, HL125816, DK124336, and AI140754, Pilot awards from the NYU CTSA grant UL1TR001445, NYU Cancer Center grant P30CA016087, and NYU Colton Center for Autoimmunity, Faculty Scholar grant from the Howard Hughes Medical Institute, Crohn's & Colitis Foundation, Burroughs Wellcome Fund PATH award, Kenneth Rainin Foundation, and industry contracts from Abbvie and Pfizer to KC, the National Science Foundation Graduate Research Fellowship and the NRSA T32 training grant (T32AI007539) to SJG, DK088199 to RB, R35 HL139930 and R01 AI120033 to JK and DK052230 to VWY.

DECLARATION OF INTERESTS

KC receives research funding from Pfizer, Takeda, and Abbvie; has consulted for or received an honorarium from Puretech Health, Genentech, and Abbvie; and holds U.S. patent 10,722,600 and provisional patent 62/935,035. SLG consults for Aclaris Therapeutics and Eli Lilly.

References

Adolph TE, Tomczak MF, Niederreiter L, Ko HJ, Bock J, Martinez-Naves E, Glickman JN, Tschurtschenthaler M, Hartwig J, Hosomi S, et al. (2013). Paneth cells as a site of origin for intestinal inflammation. Nature 503, 272–276. [PubMed: 24089213]

Ali AK, Torosian A, Porter C, Bloomfeld RS, and Feldman SR (2021). New Onset Inflammatory Bowel Disease in Patient Treated with Secukinumab: Case Report and Review of Literature. Dermatol Ther.

Amatya N, Garg AV, and Gaffen SL (2017). IL-17 Signaling: The Yin and the Yang. Trends Immunol 38, 310–322. [PubMed: 28254169]

Ayyaz A, Kumar S, Sangiorgi B, Ghoshal B, Gosio J, Ouladan S, Fink M, Barutcu S, Trcka D, Shen J, et al. (2019). Single-cell transcriptomes of the regenerating intestine reveal a revival stem cell. Nature 569, 121–125. [PubMed: 31019301]

Barker N, and Clevers H (2010). Leucine-rich repeat-containing G-protein-coupled receptors as markers of adult stem cells. Gastroenterology 138, 1681–1696. [PubMed: 20417836]

Bastide P, Darido C, Pannequin J, Kist R, Robine S, Marty-Double C, Bibeau F, Scherer G, Joubert D, Hollande F, et al. (2007). Sox9 regulates cell proliferation and is required for Paneth cell differentiation in the intestinal epithelium. J Cell Biol 178, 635–648. [PubMed: 17698607]

Borten MA, Bajikar SS, Sasaki N, Clevers H, and Janes KA (2018). Automated brightfield morphometry of 3D organoid populations by OrganoSeg. Sci Rep 8, 5319. [PubMed: 29593296]

Cadwell K, Liu JY, Brown SL, Miyoshi H, Loh J, Lennerz JK, Kishi C, Kc W, Carrero JA, Hunt S, et al. (2008). A key role for autophagy and the autophagy gene Atg16l1 in mouse and human intestinal Paneth cells. Nature 456, 259–263. [PubMed: 18849966]

Cadwell K, Patel KK, Maloney NS, Liu TC, Ng AC, Storer CE, Head RD, Xavier R, Stappenbeck TS, and Virgin HW (2010). Virus-plus-susceptibility gene interaction determines Crohn's disease gene Atg16L1 phenotypes in intestine. Cell 141, 1135–1145. [PubMed: 20602997]

Castillo-Azofeifa D, Fazio EN, Nattiv R, Good HJ, Wald T, Pest MA, de Sauvage FJ, Klein OD, and Asfaha S (2019). Atoh1(+) secretory progenitors possess renewal capacity independent of Lgr5(+) cells during colonic regeneration. EMBO J.

Durand A, Donahue B, Peignon G, Letourneur F, Cagnard N, Slomianny C, Perret C, Shroyer NF, and Romagnolo B (2012). Functional intestinal stem cells after Paneth cell ablation induced by the loss of transcription factor Math1 (Atoh1). Proceedings of the National Academy of Sciences 109, 8965–8970.

Farin HF, Van Es JH, and Clevers H (2012). Redundant sources of Wnt regulate intestinal stem cells and promote formation of Paneth cells. Gastroenterology 143, 1518–1529 e1517. [PubMed: 22922422]

Fauny M, Moulin D, D'Amico F, Netter P, Petitpain N, Arnone D, Jouzeau JY, Loeuille D, and Peyrin-Biroulet L (2020). Paradoxical gastrointestinal effects of interleukin-17 blockers. Ann Rheum Dis 79, 1132–1138. [PubMed: 32719044]

Frantz AL, Rogier EW, Weber CR, Shen L, Cohen DA, Fenton LA, Bruno ME, and Kaetzel CS (2012). Targeted deletion of MyD88 in intestinal epithelial cells results in compromised antibacterial immunity associated with downregulation of polymeric immunoglobulin receptor, mucin-2, and antibacterial peptides. Mucosal Immunol 5, 501–512. [PubMed: 22491177]

Fujii M, Matano M, Toshimitsu K, Takano A, Mikami Y, Nishikori S, Sugimoto S, and Sato T (2018). Human Intestinal Organoids Maintain Self-Renewal Capacity and Cellular Diversity in Niche-Inspired Culture Condition. Cell Stem Cell 23, 787–793 e786. [PubMed: 30526881]

Fujii M, and Sato T (2020). Somatic cell-derived organoids as prototypes of human epithelial tissues and diseases. Nat Mater.

Gaudino SJ, Beaupre M, Lin X, Joshi P, Rathi S, McLaughlin PA, Kempen C, Mehta N, Eskiocak O, Yueh B, et al. (2020). IL-22 receptor signaling in Paneth cells is critical for their maturation, microbiota colonization, Th17-related immune responses, and anti-Salmonella immunity. Mucosal Immunol.

Gerbe F, van Es JH, Makrini L, Brulin B, Mellitzer G, Robine S, Romagnolo B, Shroyer NF, Bourgaux JF, Pignodel C, et al. (2011). Distinct ATOH1 and Neurog3 requirements define tuft cells as a new secretory cell type in the intestinal epithelium. J Cell Biol 192, 767–780. [PubMed: 21383077]

Gordon KB, Blauvelt A, Papp KA, Langley RG, Luger T, Ohtsuki M, Reich K, Amato D, Ball SG, Braun DK, et al. (2016). Phase 3 Trials of Ixekizumab in Moderate-to-Severe Plaque Psoriasis. N Engl J Med 375, 345–356. [PubMed: 27299809]

Gracz AD, Samsa LA, Fordham MJ, Trotier DC, Zwarycz B, Lo YH, Bao K, Starmer J, Raab JR, Shroyer NF, et al. (2018). Sox4 Promotes Atoh1-Independent Intestinal Secretory Differentiation Toward Tuft and Enteroendocrine Fates. Gastroenterology 155, 1508–1523 e1510. [PubMed: 30055169]

Gregorieff A, Pinto D, Begthel H, Destree O, Kielman M, and Clevers H (2005). Expression pattern of Wnt signaling components in the adult intestine. Gastroenterology 129, 626–638. [PubMed: 16083717]

Gunther C, Martini E, Wittkopf N, Amann K, Weigmann B, Neumann H, Waldner MJ, Hedrick SM, Tenzer S, Neurath MF, and Becker C (2011). Caspase-8 regulates TNF-alpha-induced epithelial necroptosis and terminal ileitis. Nature 477, 335–339. [PubMed: 21921917]

Haber AL, Biton M, Rogel N, Herbst RH, Shekhar K, Smillie C, Burgin G, Delorey TM, Howitt MR, Katz Y, et al. (2017). A single-cell survey of the small intestinal epithelium. Nature 551, 333–339. [PubMed: 29144463]

Hueber W, Sands BE, Lewitzky S, Vandemeulebroecke M, Reinisch W, Higgins PD, Wehkamp J, Feagan BG, Yao MD, Karczewski M, et al. (2012). Secukinumab, a human anti-IL-17A

monoclonal antibody, for moderate to severe Crohn's disease: unexpected results of a randomised, double-blind placebo-controlled trial. Gut 61, 1693–1700. [PubMed: 22595313]

Hyun YS, Han DS, Lee AR, Eun CS, Youn J, and Kim HY (2012). Role of IL-17A in the development of colitis-associated cancer. Carcinogenesis 33, 931–936. [PubMed: 22354874]

Ishibashi F, Shimizu H, Nakata T, Fujii S, Suzuki K, Kawamoto A, Anzai S, Kuno R, Nagata S, Ito G, et al. (2018). Contribution of ATOH1(+) Cells to the Homeostasis, Repair, and Tumorigenesis of the Colonic Epithelium. Stem Cell Reports 10, 27–42. [PubMed: 29233556]

Kumar P, Monin L, Castillo P, Elsegeiny W, Horne W, Eddens T, Vikram A, Good M, Schoenborn Alexi A., Bibby K, et al. (2016). Intestinal Interleukin-17 Receptor Signaling Mediates Reciprocal Control of the Gut Microbiota and Autoimmune Inflammation. Immunity 44, 659–671. [PubMed: 26982366]

Langley RG, Elewski BE, Lebwohl M, Reich K, Griffiths CE, Papp K, Puig L, Nakagawa H, Spelman L, Sigurgeirsson B, et al. (2014). Secukinumab in plaque psoriasis--results of two phase 3 trials. N Engl J Med 371, 326–338. [PubMed: 25007392]

Lee Jacob S., Tato Cristina M., Joyce-Shaikh B, Gulan F, Cayatte C, Chen Y, Blumenschein Wendy M., Judo M, Ayanoglu G, McClanahan Terrill K., et al. (2015). Interleukin-23-Independent IL-17 Production Regulates Intestinal Epithelial Permeability. Immunity 43, 727–738. [PubMed: 26431948]

Li Y, Liu Y, Liu B, Wang J, Wei S, Qi Z, Wang S, Fu W, and Chen YG (2018). A growth factor-free culture system underscores the coordination between Wnt and BMP signaling in Lgr5(+) intestinal stem cell maintenance. Cell Discov 4, 49. [PubMed: 30181900]

Liu TC, Gurram B, Baldridge MT, Head R, Lam V, Luo C, Cao Y, Simpson P, Hayward M, Holtz ML, et al. (2016). Paneth cell defects in Crohn's disease patients promote dysbiosis. JCI Insight 1, e86907. [PubMed: 27699268]

Lo YH, Chung E, Li Z, Wan YW, Mahe MM, Chen MS, Noah TK, Bell KN, Yalamanchili HK, Klisch TJ, et al. (2017). Transcriptional Regulation by ATOH1 and its Target SPDEF in the Intestine. Cell Mol Gastroenterol Hepatol 3, 51–71. [PubMed: 28174757]

Mah AT, Yan KS, and Kuo CJ (2016). Wnt pathway regulation of intestinal stem cells. J Physiol 594, 4837–4847. [PubMed: 27581568]

Mao K, Baptista AP, Tamoutounour S, Zhuang L, Bouladoux N, Martins AJ, Huang Y, Gerner MY, Belkaid Y, and Germain RN (2018). Innate and adaptive lymphocytes sequentially shape the gut microbiota and lipid metabolism. Nature 554, 255–259. [PubMed: 29364878]

Marchiando AM, Ramanan D, Ding Y, Gomez LE, Hubbard-Lucey VM, Maurer K, Wang C, Ziel JW, van Rooijen N, Nunez G, et al. (2013). A deficiency in the autophagy gene Atg16L1 enhances resistance to enteric bacterial infection. Cell Host Microbe 14, 216–224. [PubMed: 23954160]

Martin PK, Marchiando A, Xu R, Rudensky E, Yeung F, Schuster SL, Kernbauer E, and Cadwell K (2018). Autophagy proteins suppress protective type I interferon signalling in response to the murine gut microbiota. Nat Microbiol 3, 1131–1141. [PubMed: 30202015]

Matsuzawa-Ishimoto Y, Hine A, Shono Y, Rudensky E, Lazrak A, Yeung F, Neil JA, Yao X, Chen YH, Heaney T, et al. (2020). An intestinal organoid-based platform that recreates susceptibility to T-cell-mediated tissue injury. Blood 135, 2388–2401. [PubMed: 32232483]

Matsuzawa-Ishimoto Y, Shono Y, Gomez LE, Hubbard-Lucey VM, Cammer M, Neil J, Dewan MZ, Lieberman SR, Lazrak A, Marinis JM, et al. (2017). Autophagy protein ATG16L1 prevents necroptosis in the intestinal epithelium. J Exp Med 214, 3687–3705. [PubMed: 29089374]

Maxwell Joseph R., Zhang Y, Brown William A., Smith Carole L., Byrne Fergus R., Fiorino M, Stevens E, Bigler J, Davis John A., Rottman James B., et al. (2015). Differential Roles for Interleukin-23 and Interleukin-17 in Intestinal Immunoregulation. Immunity 43, 739–750. [PubMed: 26431947]

McGeachy MJ, Cua DJ, and Gaffen SL (2019). The IL-17 Family of Cytokines in Health and Disease. Immunity 50, 892–906. [PubMed: 30995505]

Middendorp S, Schneeberger K, Wiegerinck CL, Mokry M, Akkerman RD, van Wijngaarden S, Clevers H, and Nieuwenhuis EE (2014). Adult stem cells in the small intestine are intrinsically programmed with their location-specific function. Stem Cells 32, 1083–1091. [PubMed: 24496776]

Miyoshi H, and Stappenbeck TS (2013). In vitro expansion and genetic modification of gastrointestinal stem cells in spheroid culture. Nat Protoc 8, 2471–2482. [PubMed: 24232249]

Mu X, Fardy J, Reid S, and Trahey J (2021). Severe drug-associated colitis with Crohn's features in setting of ixekizumab therapy for chronic plaque psoriasis. BMC Gastroenterol 21, 361. [PubMed: 34600483]

Nanki K, Fujii M, Shimokawa M, Matano M, Nishikori S, Date S, Takano A, Toshimitsu K, Ohta Y, Takahashi S, et al. (2020). Somatic inflammatory gene mutations in human ulcerative colitis epithelium. Nature 577, 254–259. [PubMed: 31853059]

Neil JA, Matsuzawa-Ishimoto Y, Kernbauer-Holzl E, Schuster SL, Sota S, Venzon M, Dallari S, Galvao Neto A, Hine A, Hudesman D, et al. (2019). IFN-I and IL-22 mediate protective effects of intestinal viral infection. Nat Microbiol 4, 1737–1749. [PubMed: 31182797]

Onishi RM, and Gaffen SL (2010). Interleukin-17 and its target genes: mechanisms of interleukin-17 function in disease. Immunology 129, 311–321. [PubMed: 20409152]

Oshiro K, Kohama H, Umemura M, Uyttenhove C, Inagaki-Ohara K, Arakawa T, Harada M, Nakae S, Iwakura Y, Nishimaki T, and Matsuzaki G (2012). Interleukin-17A is involved in enhancement of tumor progression in murine intestine. Immunobiology 217, 54–60. [PubMed: 21962571]

Papp KA, Leonardi C, Menter A, Ortonne JP, Krueger JG, Kricorian G, Aras G, Li J, Russell CB, Thompson EH, and Baumgartner S (2012). Brodalumab, an anti-interleukin-17-receptor antibody for psoriasis. N Engl J Med 366, 1181–1189. [PubMed: 22455412]

Ramanan D, and Cadwell K (2016). Intrinsic Defense Mechanisms of the Intestinal Epithelium. Cell Host Microbe 19, 434–441. [PubMed: 27049583]

Salzman NH (2010). Paneth cell defensins and the regulation of the microbiome: Détente at mucosal surfaces. Gut Microbes 1, 401–406. [PubMed: 21468224]

Sato T, Stange DE, Ferrante M, Vries RG, Van Es JH, Van den Brink S, Van Houdt WJ, Pronk A, Van Gorp J, Siersema PD, and Clevers H (2011a). Long-term expansion of epithelial organoids from human colon, adenoma, adenocarcinoma, and Barrett's epithelium. Gastroenterology 141, 1762–1772. [PubMed: 21889923]

Sato T, van Es JH, Snippert HJ, Stange DE, Vries RG, van den Born M, Barker N, Shroyer NF, van de Wetering M, and Clevers H (2011b). Paneth cells constitute the niche for Lgr5 stem cells in intestinal crypts. Nature 469, 415–418. [PubMed: 21113151]

Sato T, Vries RG, Snippert HJ, van de Wetering M, Barker N, Stange DE, van Es JH, Abo A, Kujala P, Peters PJ, and Clevers H (2009). Single Lgr5 stem cells build crypt-villus structures in vitro without a mesenchymal niche. Nature 459, 262–265. [PubMed: 19329995]

Schmitt M, Schewe M, Sacchetti A, Feijtel D, van de Geer WS, Teeuwssen M, Sleddens HF, Joosten R, van Royen ME, van de Werken HJG, et al. (2018). Paneth Cells Respond to Inflammation and Contribute to Tissue Regeneration by Acquiring Stem-like Features through SCF/c-Kit Signaling. Cell Rep 24, 2312–2328 e2317. [PubMed: 30157426]

Schwarzenberger P, La Russa V, Miller A, Ye P, Huang W, Zieske A, Nelson S, Bagby GJ, Stoltz D, Mynatt RL, et al. (1998). IL-17 Stimulates Granulopoiesis in Mice: Use of an Alternate, Novel Gene Therapy-Derived Method for In Vivo Evaluation of Cytokines. The Journal of Immunology 161, 6383–6389. [PubMed: 9834129]

Shen F, Hu Z, Goswami J, and Gaffen SL (2006). Identification of common transcriptional regulatory elements in interleukin-17 target genes. J Biol Chem 281, 24138–24148. [PubMed: 16798734]

Song X, Dai D, He X, Zhu S, Yao Y, Gao H, Wang J, Qu F, Qiu J, Wang H, et al. (2015). Growth Factor FGF2 Cooperates with Interleukin-17 to Repair Intestinal Epithelial Damage. Immunity 43, 488–501. [PubMed: 26320657]

Targan SR, Feagan B, Vermeire S, Panaccione R, Melmed GY, Landers C, Li D, Russell C, Newmark R, Zhang N, et al. (2016). A Randomized, Double-Blind, Placebo-Controlled Phase 2 Study of Brodalumab in Patients With Moderate-to-Severe Crohn's Disease. Am J Gastroenterol 111, 1599–1607. [PubMed: 27481309]

Thorne CA, Chen IW, Sanman LE, Cobb MH, Wu LF, and Altschuler SJ (2018). Enteroid Monolayers Reveal an Autonomous WNT and BMP Circuit Controlling Intestinal Epithelial Growth and Organization. Dev Cell 44, 624–633 e624. [PubMed: 29503158]

Tomic G, Morrissey E, Kozar S, Ben-Moshe S, Hoyle A, Azzarelli R, Kemp R, Chilamakuri CSR, Itzkovitz S, Philpott A, and Winton DJ (2018). Phospho-regulation of ATOH1 Is Required for Plasticity of Secretory Progenitors and Tissue Regeneration. Cell Stem Cell 23, 436–443 e437. [PubMed: 30100168]

Vaishnava S, Behrendt CL, Ismail AS, Eckmann L, and Hooper LV (2008). Paneth cells directly sense gut commensals and maintain homeostasis at the intestinal host-microbial interface. Proceedings of the National Academy of Sciences of the United States of America 105, 20858–20863. [PubMed: 19075245]

VanDussen KL, Liu TC, Li D, Towfic F, Modiano N, Winter R, Haritunians T, Taylor KD, Dhall D, Targan SR, et al. (2014). Genetic variants synthesize to produce paneth cell phenotypes that define subtypes of Crohn's disease. Gastroenterology 146, 200–209. [PubMed: 24076061]

von Moltke J, Ji M, Liang HE, and Locksley RM (2016). Tuft-cell-derived IL-25 regulates an intestinal ILC2-epithelial response circuit. Nature 529, 221–225. [PubMed: 26675736]

Wang K, Kim MK, Di Caro G, Wong J, Shalapour S, Wan J, Zhang W, Zhong Z, Sanchez-Lopez E, Wu LW, et al. (2014). Interleukin-17 receptor a signaling in transformed enterocytes promotes early colorectal tumorigenesis. Immunity 41, 1052–1063. [PubMed: 25526314]

Wright MC, Reed-Geaghan EG, Bolock AM, Fujiyama T, Hoshino M, and Maricich SM (2015). Unipotent, Atoh1+ progenitors maintain the Merkel cell population in embryonic and adult mice. J Cell Biol 208, 367–379. [PubMed: 25624394]

Wu S, Rhee KJ, Albesiano E, Rabizadeh S, Wu X, Yen HR, Huso DL, Brancati FL, Wick E, McAllister F, et al. (2009). A human colonic commensal promotes colon tumorigenesis via activation of T helper type 17 T cell responses. Nat Med 15, 1016–1022. [PubMed: 19701202]

Yang Q, Bermingham NA, Finegold MJ, and Zoghbi HY (2001). Requirement of Math1 for secretory cell lineage commitment in the mouse intestine. Science 294, 2155–2158. [PubMed: 11739954]

Yin X, Farin HF, van Es JH, Clevers H, Langer R, and Karp JM (2014). Niche-independent high-purity cultures of Lgr5+ intestinal stem cells and their progeny. Nat Methods 11, 106–112. [PubMed: 24292484]

Zha JM, Li HS, Lin Q, Kuo WT, Jiang ZH, Tsai PY, Ding N, Wu J, Xu SF, Wang YT, et al. (2019). Interleukin 22 Expands Transit-Amplifying Cells While Depleting Lgr5(+) Stem Cells via Inhibition of Wnt and Notch Signaling. Cell Mol Gastroenterol Hepatol 7, 255–274. [PubMed: 30686779]

Highlights:

- Generated different intestinal epithelial cell-specific *Il17ra*-deficient mouse lines.
- IL-17A acts on $Lgr5^+$ ISCs to promote secretory cell lineage commitment.
- *Il17ra* deficiency in $ATOH1^+$ cells exacerbates DSS-induced colitis.
- IL-17A stimulates secretory cell differentiation in cystic human intestinal organoids.

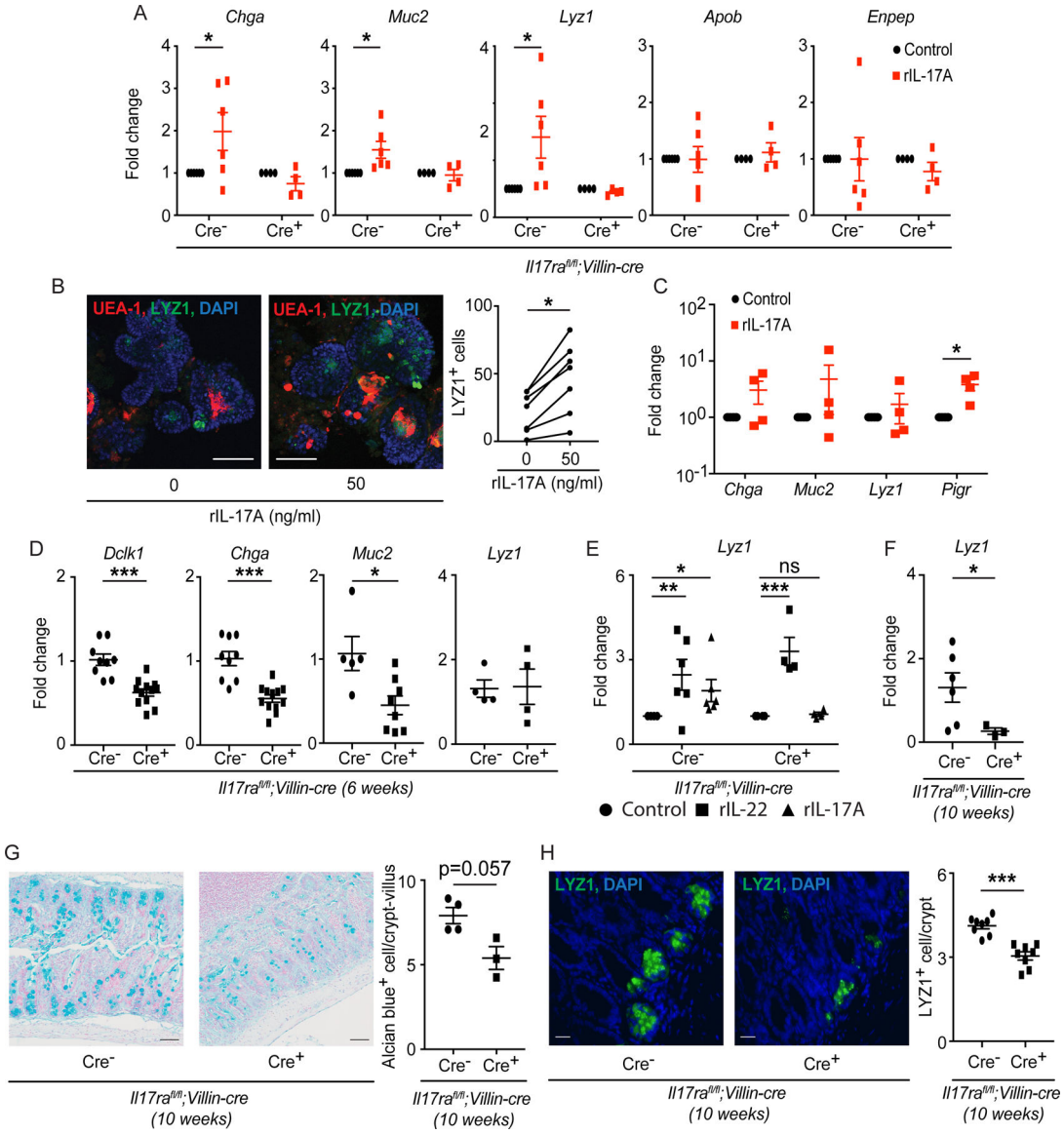

Figure 1. Secretory cell defects occur in the absence of intestinal IL-17RA.

A) Crypts were isolated from the ileum of *Il17ra*$^{fl/fl}$*;Villin-cre* mice and used for organoid culture. RT-PCR data depict the expression of *Chga, Muc2*, *Lyz1, Apob and Enpep* after recombinant IL-17A treatment (50 ng/ml). **B)** Crypts were isolated from the ileum of C57BL/6J ATOH1-EGFP mice and used for organoid culture in the presence of recombinant IL-17A (50 ng/ml). Immunofluorescence was used to analyze LYZ1^{+} cells and cells bound by UEA-1 (left panel). The number of LYZ1^{+} cells was plotted (right panel). **C)** Crypts were isolated from the ileum of C57BL/6J *Il17ra*$^{fl/fl}$ mice and used for organoid culture. On day 5, recombinant IL-17A (50 ng/ml) or 1× PBS was added and organoids were harvested after 7 hours. RT-PCR data depict the fold change of *Chga, Muc2*, *Lyz1 and Pigr* under rIL-17A treatment as compared to untreated organoids. **D)** RNA was extracted from the terminal ileum of naïve *Il17ra*$^{fl/fl}$*;Villin-cre* mice at 6 weeks old. RT-PCR data depict the expression of *Dclk1, Chga, Muc2* and *Lyz1*. **E)** Crypts were isolated from the ileum

of *Il17ra*$^{fl/fl}$*;Villin-cre* mice and used for organoid culture under recombinant IL-17A (50 ng/ml) or IL-22 (10 ng/ml) treatment. RT-PCR data depict the expression of *Lyz1*. **F)** RNA was extracted from the terminal ileum of naïve *Il17ra*$^{fl/fl}$*;Villin-cre* mice at 10 weeks old. RT-PCR data depict the expression of *Lyz1*. **G)** The terminal ileum of *Il17ra*$^{fl/fl}$*;Villin-cre* mice was harvested at 10 weeks old and stained with alcian blue (top panel). The number of alcian blue^{+} cells was plotted (bottom panel). **H)** The terminal ileum of *Il17ra*$^{fl/fl}$*;Villin-cre* mice was harvested at 10 weeks old and stained with anti-LYZ1 (top panel). The number of LYZ1^{+} cell/crypt was plotted (bottom panel).

Figure 1A, 1C–1F were generated from 2–3 independent experiments. Figure 1B, 1G and 1H represent at least 3 mice in each group. Data are presented as mean ± SEM in all graphs. Scale bars in relevant figures equal 100 μm (1B), 50 μm (1G) and 20 μm (1H). *$P \leq 0.05$; **$P \leq 0.01$; ***$P \leq 0.001$ (Two-Way ANOVA in A and E, paired t test in B and C, Mann-Whitney test, two-tailed in D and F-H). See also Figure S1.

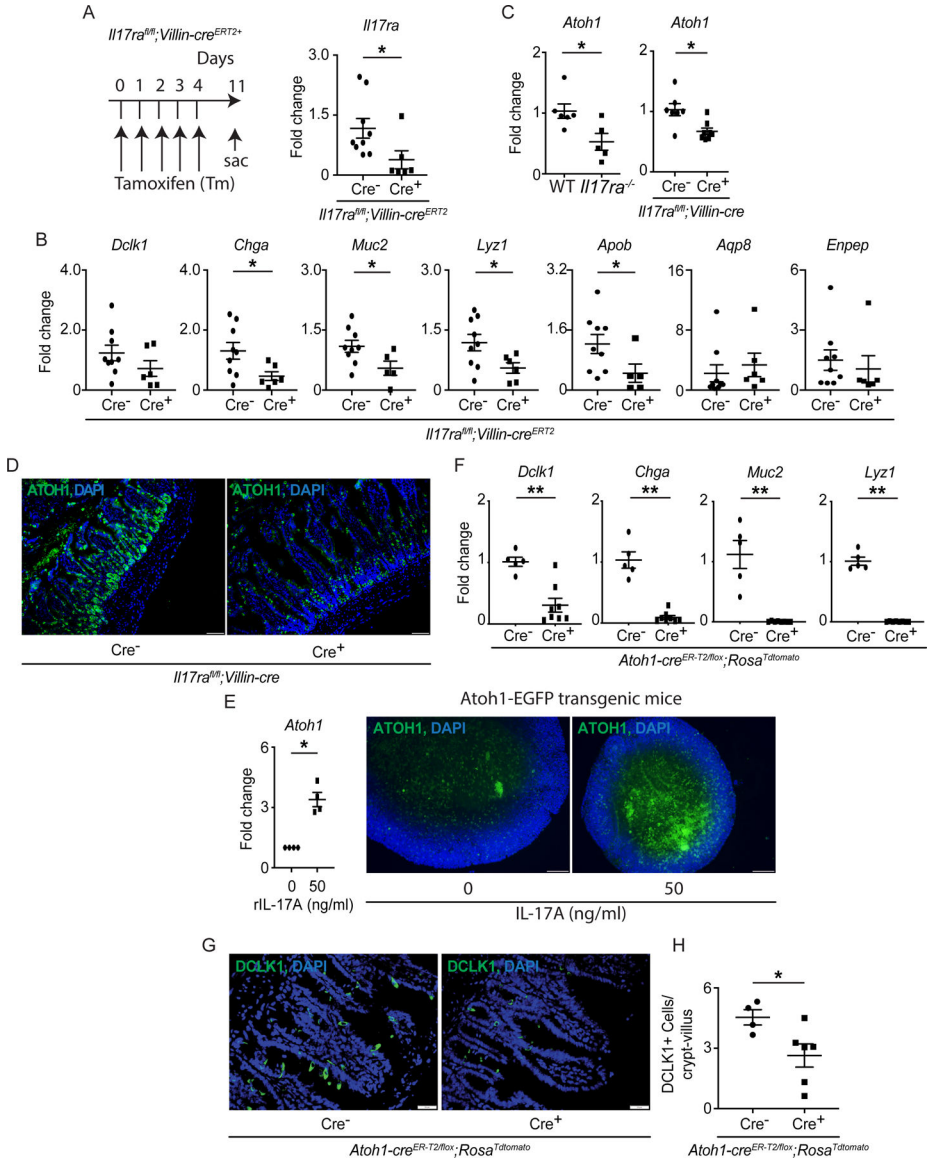

Figure 2. Mice deficient in IL-17RA display ATOH1 defects.

A-B) *Il17ra*$^{fl/fl}$*;Villin-cre*^{ERT2} mice were injected with tamoxifen for 5 continuous days. The schematic diagram shows the strategy of tamoxifen administration (A, left panel). The RNA was extracted from the terminal ileum on day 11 and RT-PCR confirmed the depletion of *Il17ra* post tamoxifen injection (A, right panel). The expression of *Dclk1, Chga, Muc2, Lyz1, Apob, Aqp8 and Enpep* was analyzed by RT-PCR (B). **C-D)** RNA was extracted from the terminal ileum of naïve WT, *Il17ra*$^{-/-}$ and *Il17ra*$^{fl/fl}$*;Villin*-cre mice. The expression of *Atoh1* was analyzed by RT-PCR (C). The terminal ileum of naïve *Il17ra*$^{fl/fl}$*;Villin-cre* mice was stained with anti-ATOH1 (D). **E)** Crypts isolated from the ileum of ATOH1-EGFP mice were used for organoid culture under recombinant IL-17A (50 ng/ml) treatment. RT-PCR was utilized to analyze the expression of *Atoh1* (left panel) and immunofluorescence showed the ATOH1 expression in the vehicle or recombinant IL-17A-treated organoids (right panel). **F-H)** The RNA was extracted from the terminal ileum

of *Atoh1-cre*$^{ER\text{-}T2/flox}$;*Rosa*^{Tdtomato} mice at one week post the last tamoxifen injection. RT-PCR data depict the expression of *Dclk1, Chga, Muc2* and *Lyz1* (F). The ileum was stained with anti-DCLK1 (G) and the number of DCLK1^{+} cells was plotted (H). Figures 2A (right panel), 2B, 2C (right panel), 2F and 2H were generated from 2–3 independent experiments. Figure 2D, 2E (right panel) and 2G are the representative images of at least 4 mice in each group. Data are presented as mean ± SEM in all graphs. Scale bars in relevant figures equal 20 μm (2D), 50 μm (2E) and 20 μm (2G). *$P \leq 0.05$; **$P \leq 0.01$ (Mann-Whitney test, two-tailed in A-C, E, F and H). See also Figure S2.

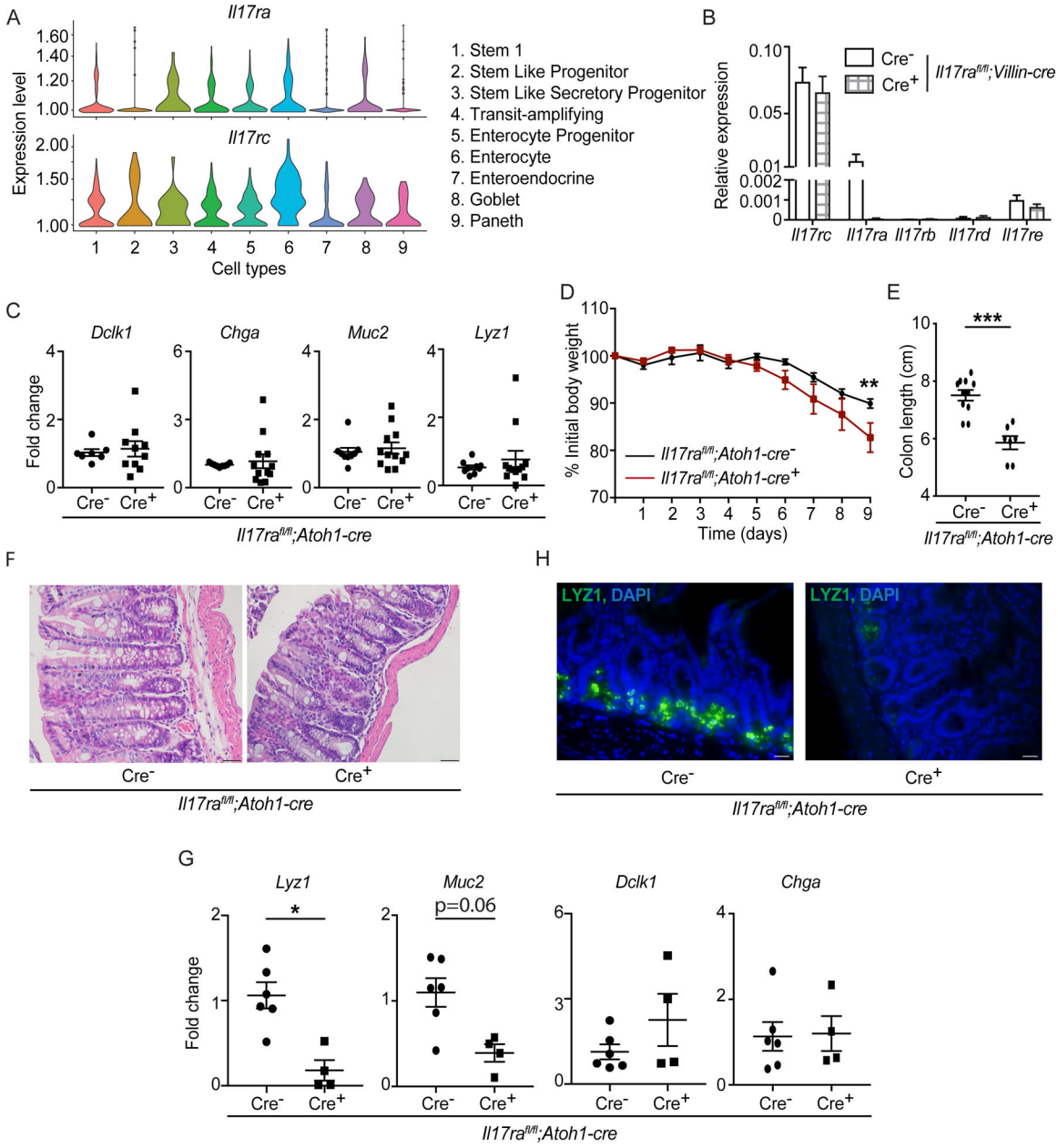

Figure 3. IL-17RA signaling in ATOH1^{+} cells is required for *Lyz1* expression after injury.

A) Single cell RNA-seq data of C57BL/6J primary small intestinal organoids depict the expression of *Il17ra* and *Il17rc* in different cell types. **B)** Crypts were isolated from naïve *Il17ra*$^{fl/fl}$*;Villin-cre* mice for organoid culture. RNA was extracted from the organoids on day 6 and the expression of *Il17* receptors was analyzed by RT-PCR. **C)** RT-PCR data depict the expression of *Dclk1, Chga, Muc2* and *Lyz1* in the terminal ileum of naïve *Il17ra*$^{fl/fl}$*;Atoh1-cre* mice at 6 weeks old. **D-H)** *Il17ra*$^{fl/fl}$*;Atoh1-cre* mice were treated with 2.5% DSS from day 0 to day 8 followed by 1 day of water. The weight was recorded daily (D). Mice were euthanized and colon length was measured on day 9 (E). Distal colon tissues were stained with hematoxylin and eosin (F). RT-PCR depict the expression of *Lyz1, Muc2,*

Dclk1 and *Chga* in the terminal ileum (G). LYZ1^{+} cells in the terminal ileum were analyzed by immunofluorescence (H).

Figures 3B, 3C, 3D, 3E and 3G were generated from 2–3 independent experiments. Figure 3F and 3H are representative of at least 3 mice in each group. Data are presented as mean ± SEM in all graphs. Scale bars in relevant figures equal 20 μm (3F) and 10 μm (3H). *$P \leq 0.05$; **$P \leq 0.01$; ***$P \leq 0.001$ (Mann-Whitney test, two-tailed in C, E and G, Two-Way ANOVA in B and D). See also Figures S2 and S3.

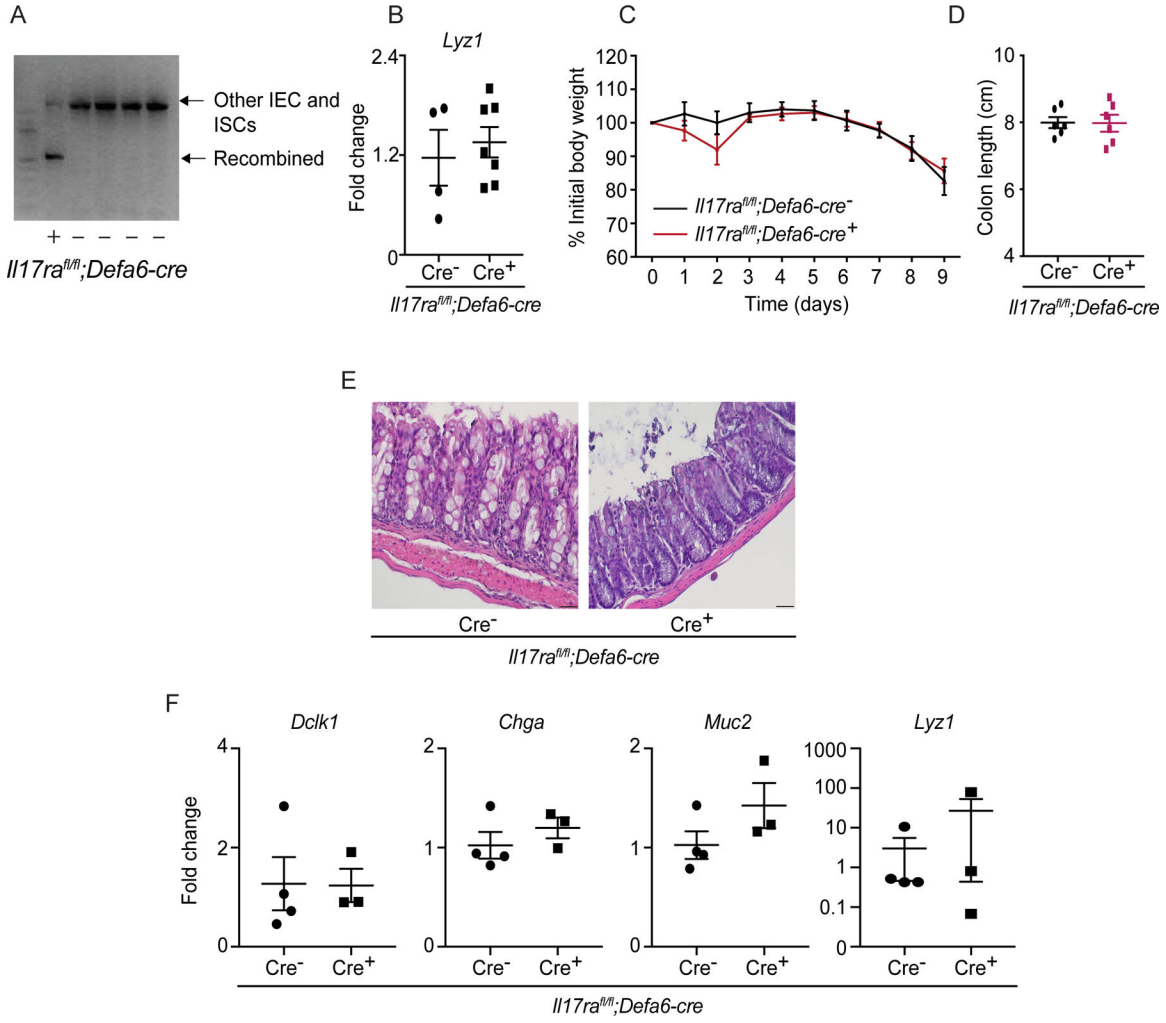

Figure 4. Paneth cell-specific IL-17RA signaling is dispensable for secretory cell regulation and DSS colitis.

A) Agarose gel confirms recombination of the IL-17RA allele in the ileum of naïve *Il17ra*$^{fl/fl}$*;Defa6-cre* mice. **B)** RNA was extracted from the terminal ileum of naïve *Il17ra*$^{fl/fl}$*;Defa6-cre* mice. The expression of *Lyz1* was analyzed by RT-PCR. **C-F)** *Il17ra*$^{fl/fl}$*;Defa6-cre* mice were treated with 2.5% DSS from day 0 to day 8 followed by 1 day of water. The weight was recorded daily (C). Mice were euthanized and colon length was measured on day 9 (D). Distal colon tissues were stained with hematoxylin and eosin (E). RT-PCR depict the expression of *Lyz1, Muc2, Dclk1* and *Chga* in the terminal ileum (F).

Figures 4B, 4C and 4D were generated from 2 independent experiments. Figure 4E is representative of at least 3 mice in each group. Data are presented as mean ± SEM in all graphs. Scale bars in relevant figures equal 20 μm (4E). (Mann-Whitney test, two-tailed in B, D and F, Two-Way ANOVA in C).

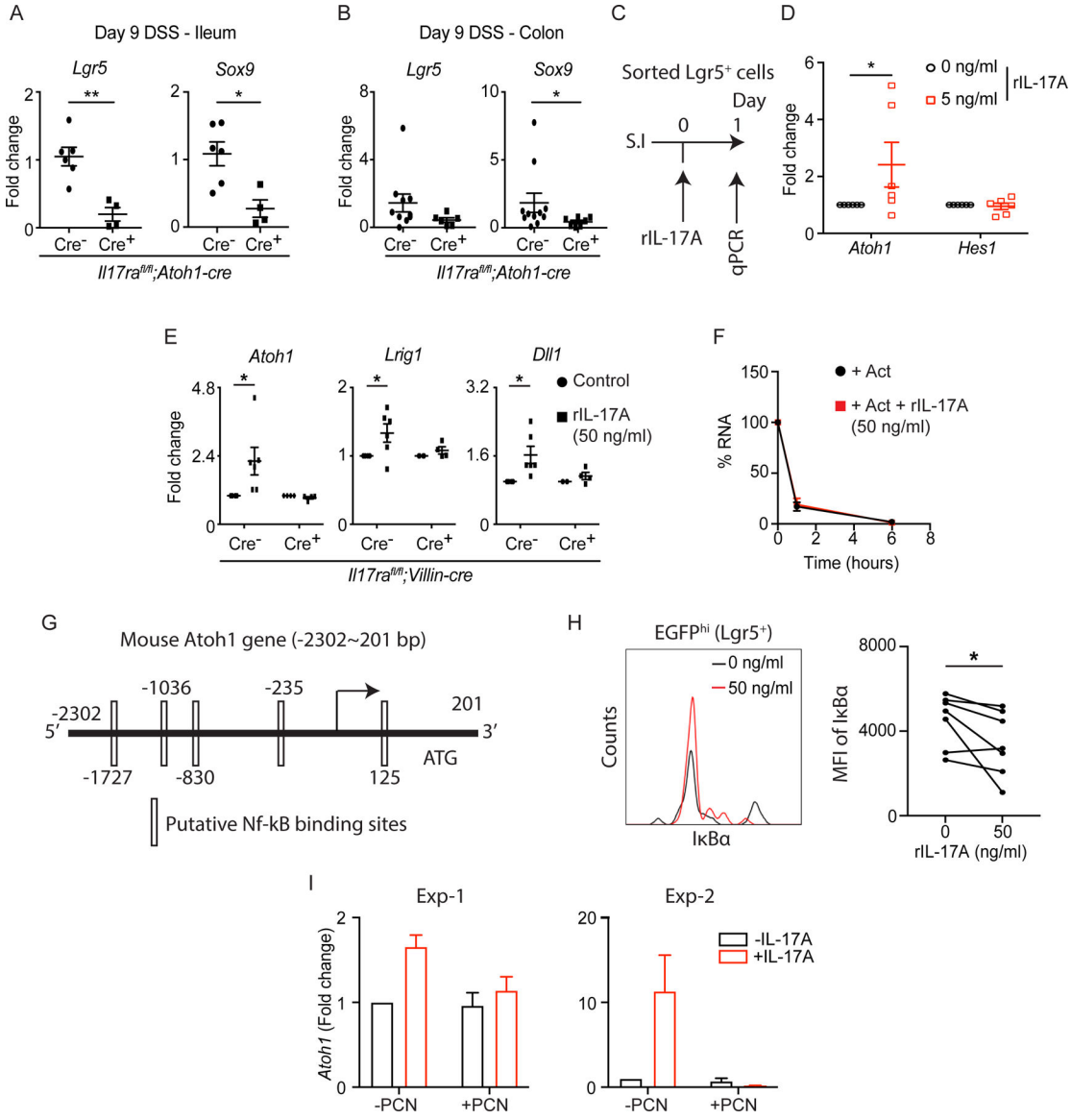

Figure 5. IL-17A signaling in Lgr5^{+} ISCs regulates ATOH1 activity in an NF-κB-dependent manner.

. A-B) *Il17ra*$^{fl/fl}$*;Atoh1-cre* mice were treated with 2.5% DSS for 8 continuous days followed by 1 day of water. RT-PCR data depict the expression of *Lgr5* and *Sox9* in the terminal ileum (A) and distal colon (B) harvested on day 9. **C-D)** Crypts were isolated from the ileum of *Lgr5-EGFP*-cre^{ERT2+} mice. EGFP^{hi} cells (Lgr5^{+} ISCs) were sorted by fluorescence-activated cell sorting (FACS). The schematic diagram shows the strategy of IL-17A treatment on sorted Lgr5^{+} ISCs (C). The expression of *Atoh1* and *Hes1* was analyzed by RT-PCR (D). **E)** Crypts isolated from the ileum of *Il17ra*$^{fl/fl}$*;Villin-cre* mice were used for organoid culture under recombinant IL-17A (50 ng/ml) treatment. The expression of *Atoh1, Lrig1* and *Dll1* was analyzed by RT-PCR. **F)** Primary C57BL/6J organoids were treated with actinomycin D (5 μg/mL) and recombinant IL-17A (50 ng/ml). *Atoh1* transcripts were quantified at the indicated time points by RT-PCR. **G)** Putative NF-κB binding motifs are predicted in the mouse *Atoh1* promoter. **H-I)** Crypts were isolated

from the ileum of *Il17ra*$^{fl/fl}$*;Lgr5-EGFP-cre*$^{ERT2+}$ mice (without tamoxifen administration) and used for primary organoid culture under the treatment of recombinant IL-17A (50 ng/ml) or piceatannol (10 μM). After 5 days of recombinant IL-17A treatment, organoids were processed for flow cytometry. Live Lgr5^{hi} cells were gated and the MFI of IκBα was plotted (H). The expression of *Atoh1* in organoids harvested after 5-day treatment of piceatannol was analyzed by RT-PCR (I).

Figures 5A, 5B, 5D, 5E, 5H and 5I were generated from 2–3 independent experiments. Figure 5F was generated from 3 mice in each group. Data are presented as mean ± SEM in all graphs. *$P \leq 0.05$; **$P \leq 0.01$ (Mann-Whitney test, two-tailed in A and B, Two-Way ANOVA in D-F, Wilcoxon matched-pairs test in H). See also Figures S4 and S5.

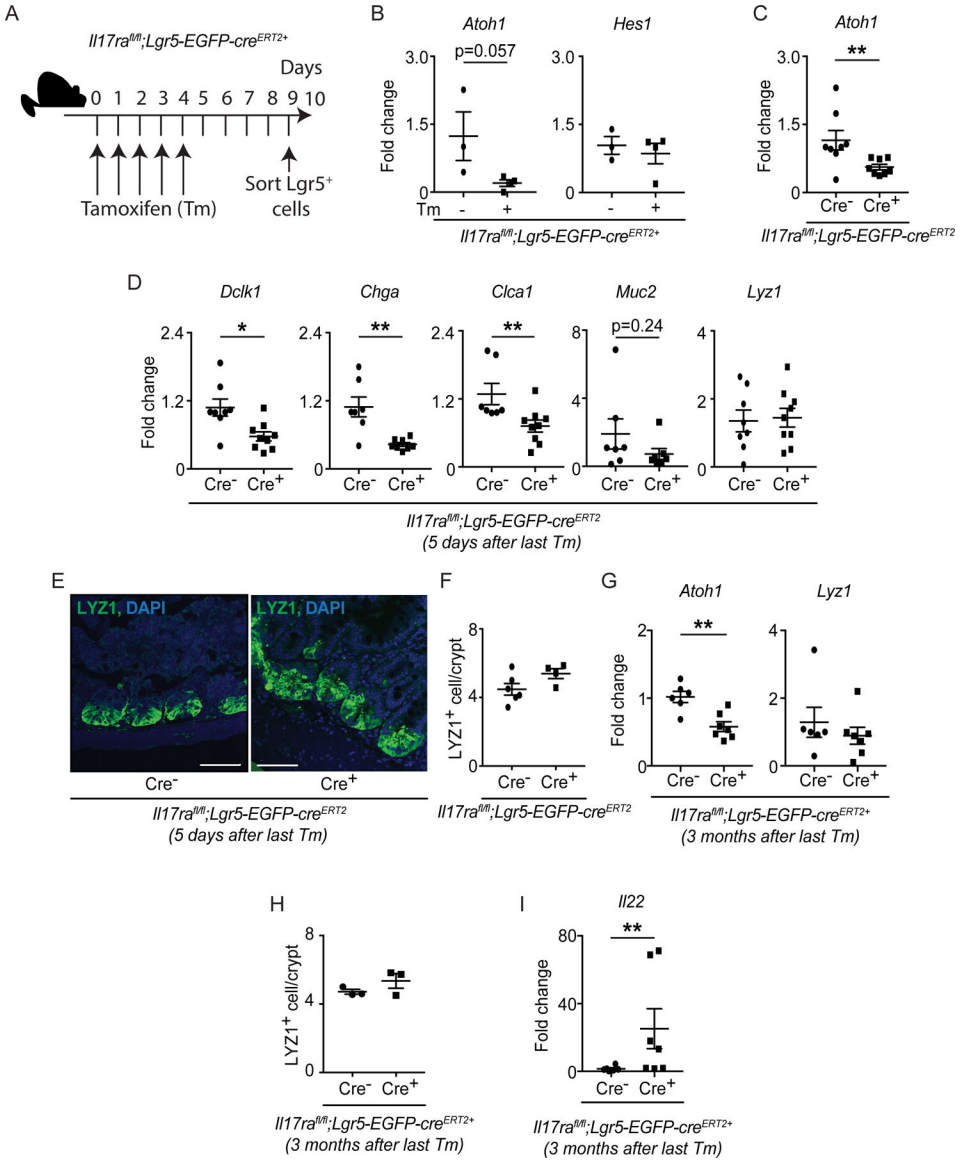

Figure 6. IL-17RA signaling in Lgr5^{+} ISCs regulates Atoh1 and the development of intestinal secretory cells.

A-B) *Il17ra*$^{fl/fl}$*;Lgr5-EGFP-cre*$^{ERT2+}$ mice were injected with tamoxifen (Tm) or corn oil for 5 continuous days. Crypts were isolated from the ileum on day 9. EGPF^{hi} cells (Lgr5^{+} ISCs) were sorted by FACS. The schematic diagram shows the strategy of tamoxifen treatment (A). The expression of *Atoh1* and *Hes1* in sorted EGFP^{hi} cells was analyzed by RT-PCR. **C-F)** *Il17ra*$^{fl/fl}$*;Lgr5-EGFP-cre*^{ERT2} mice were injected with tamoxifen for 5 continuous days. The terminal ileum was harvested on day 9 for RNA extraction. RT-PCR data depict the expression of *Atoh1* (C), *Dclk1, Chga, Clca1, Muc2* and *Lyz1* (D). The terminal ileum was stained with anti-LYZ1 (E) and the number of LYZ1^{+} cells was plotted (F)**. G-I)** *Il17ra*$^{fl/fl}$*;Lgr5-EGFP-cre*^{ERT2} mice were injected with tamoxifen for 5 continuous days. The terminal ileum was harvested at 3 months post the last tamoxifen injection for RNA extraction. RT-PCR data depict the expression of *Atoh1*, *Lyz1* (G) and *Il22* (I). Terminal ileum tissues were stained with anti-LYZ1 and the number of LYZ1^{+} cells was plotted (H).

Figures 6B, 6C, 6D, 6G and 6I were generated from 2–3 independent experiments. Figure 6F and 6H were generated from at least 3 mice in each group. Figure 6E is representative of at least 3 mice in each group. Data are presented as mean ± SEM in all graphs. Scale bars in relevant figures equal 50 μm (6E). *$P \leq 0.05$; **$P \leq 0.01$ (Mann-Whitney test, two-tailed in B-D and F-I). See also Figure S5.

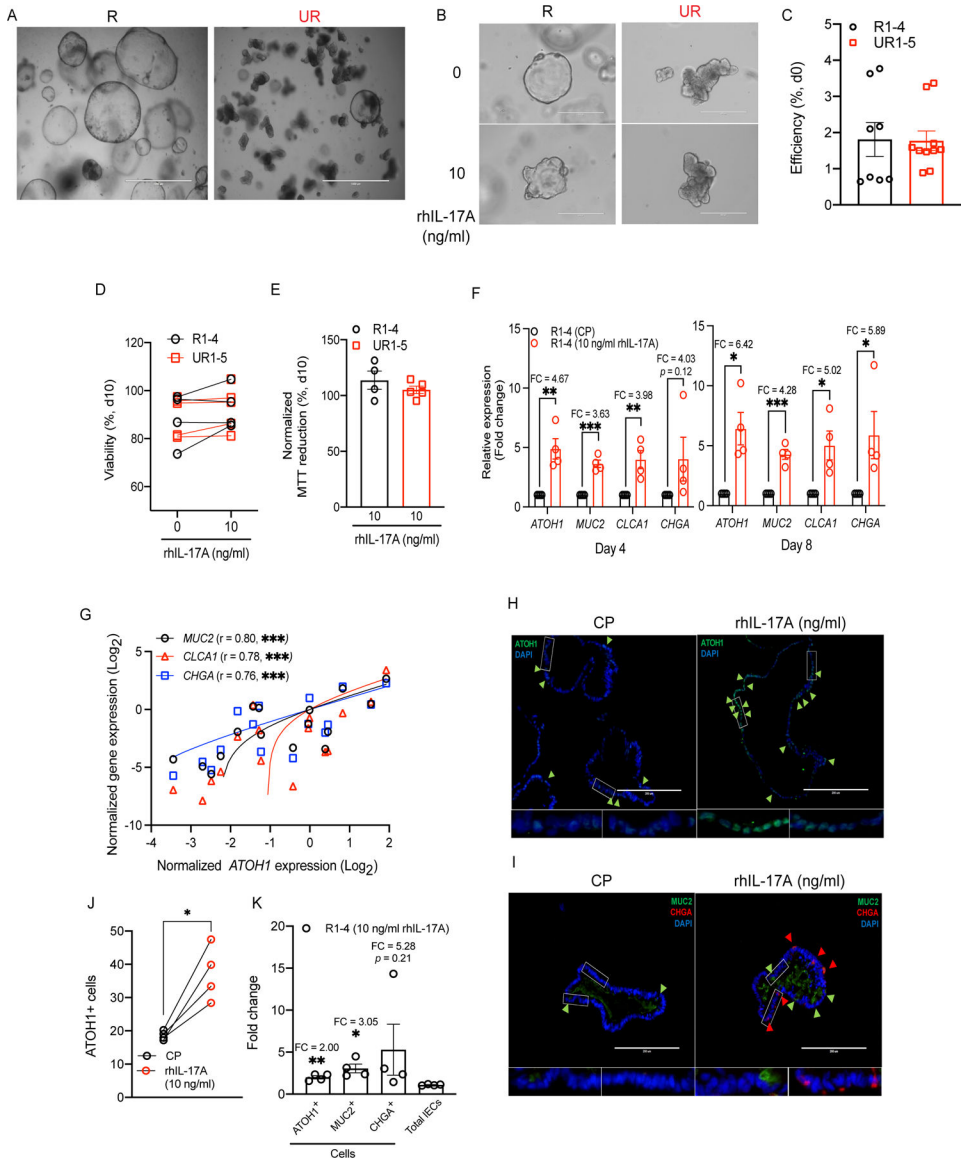

Figure 7. IL-17A-mediated rescue of secretory cell lineage defects in human intestinal organoids.

A) Representative organoid images of IL-17A-responsive (R) and -unresponsive (UR) lines grown under conventional method on day 6. **B)** Representative organoid images of the same R and UR lines from (A) on day 4 following plating single cell suspensions in the presence of rhIL-17A or carrier protein control. **C)** Organoid-forming efficiency normalized to the total number of single cells from the rhIL-17A-stimulated and -unstimulated R1–4 or UR1–5 lines on day 0. **D-E)** Viability according to visual inspection (D) and MTT reduction assay (E) of rhIL-17A-stimulated and unstimulated R or UR lines on day 10. **F)** RT-PCR data depict the fold change in *ATOH1*, *MUC2*, *CLCA1*, and *CHGA* expressions on days 4 (left) and 8 (right). **G)** Correlation of *ATOH1* expression with *MUC2*, *CLCA1*, or *CHGA* expression among the R lines on days 4 and 8. **H-I)** Representative ATOH1 staining images (H) and MUC2 and CHGA co-staining images (I) in the rhIL-17A-stimulated R lines on day 8. **J)** Total number of ATOH1^{+} cells among the rhIL-17A-stimulated R lines on day 8. **K)**

Fold change of total number of ATOH1$^+$, MUC2$^+$, or CHGA$^+$ cells, and total number of IECs among the rhIL-17A-stimulated R lines on day 8.

Data points in C-G, J and K are mean of three technical replicates of individual lines. Bars represent mean ± SEM and at least three independent experiments were performed. Bars: 1,000 μm (A); 400 μm (B); 200 μm (H and I). CP, carrier protein; FC, fold change; r, Pearson correlation coefficient. *$P \leq 0.05$; **$P \leq 0.01$; and ***$P \leq 0.001$ (unpaired t test, two-tailed in C-F and K, simple linear regression analysis in G, paired t test, two-tailed in J). See also Figures S6 and S7.

KEY RESOURCES TABLE

REAGENT or RESOURCE	SOURCE	IDENTIFIER
Antibodies		
Rabbit anti-Human Lysozyme FITC	Dako	Cat#: F037201; RRID: AB_578661
Rabbit anti-DCLK1/DCAMKL1	Cell Signaling Technology	Cat#: 62257S; RRID: AB_2799622; Clone: D2U3L
Rabbit polyclonal anti-Atoh1	Jane E Johnson UT Southwestern	N/A
Rabbit polyclonal anti-Atoh1	Proteintech	Cat#: 212151AP; RRID:AB_10733126
Rabbit anti-Ki-67	Biocare Medical	Cat#: CRM325B; Clone: SP6
Goat anti-E-cadherin	R & D	Cat#: AF748; RRID: AB_355568;
Goat anti-Lysozyme C	Santa Cruz Biotechnology	Cat#: sc-27958; RRID: AB_2138790; Clone: C-19
Mouse anti-Chr-A	Santa Cruz Biotechnology	Cat#: sc-393941; RRID: AB_2801371; Clone: C-12
Rabbit anti-Mucin 2	Santa Cruz Biotechnology	Cat#: sc-15334; RRID:AB_2146667; Clone: H-300
Mouse anti-Mucin 2	Santa Cruz Biotechnology	Cat#: sc-515032; RRID: AB_2815005; Clone: F-2
Goat anti-rabbit IgG AF488	Jackson ImmunoResearch Labs	Cat#: 111-545-144; RRID: AB_2338052
F(ab')2 goat anti-mouse IgG(H+L) AF647	Cell Signaling Technology	Cat#: 4410S; RRID: AB_ 1904023
Goat anti-Rabbit IgG (H+L) Cross-Adsorbed Secondary Antibody, Alexa Fluor 488	ThermoFisher	Cat#: A11008; RRID:AB_2536164
Goat anti-Mouse IgG (H+L), Superclonal™ Recombinant Secondary Antibody, Alexa Fluor 555	ThermoFisher	Cat#: A28180; RRID:AB_143165
APC-eFluor 780 anti-mouse CD45	eBioscience	Cat#: 47-0451-82; RRID: AB_1548781 Clone: 30-F11
PE-Cy7 anti-mouse CD3e	eBioscience	Cat#: 25-0031-82 RRID: AB_469572 Clone: 145-2C11
PE anti-mouse IL-17A	eBioscience	Cat#: 12-7177-81 RRID: AB_763582 Clone: eBio17B7
PE anti-mouse IκBα	eBioscience	Cat#: 12-9036-42 RRID: AB_2572683 Clone: MFRDTRK
Chemicals, Peptides, and Recombinant Proteins		
UEA-I Dylight 649	Vector Laboratories	Cat#: DL-1068
VECTASHIELD® HardSet™ Antifade mounting medium with DAPI	Vector Laboratories	Cat#: H-1500
ProLong™ Glass Antifade Mountant with NucBlue™ Stain	ThermoFisher	Cat#: P36981
Aqua Dead Cell Stain Kit	Invitrogen	Cat#: L34957
Recombinant mouse IL-17A	R&D Systems	Cat#: 421-ML/CF
Recombinant human IL-17A	R&D Systems	Cat#: 317-ILB-050
Recombinant mouse IL-25	R&D Systems	Cat#: 1399-IL/CF
Recombinant mouse IL-22	R&D Systems	Cat#: 582-ML
SsoAdvanced™ Universal Probes Supermix	Bio-Rad	Cat#: 1725281
SsoAdvanced™ Universal SYBR® Green Supermix	Bio-Rad	Cat#: 1725271
iScript™ Reverse Transcription Supermix	Bio-Rad	Cat#: 1708840

REAGENT or RESOURCE	SOURCE	IDENTIFIER
High-Capacity cDNA Reverse Transcription Kit	ThermoFisher	Cat#: 4368814
Roche Diagnostics LIGHTCYCLER 480 SYBR GREEN	Roche	Cat#: 04887352001
Actinomycin D	Sigma-Aldrich	Cat#: A9415
Piceatannol	EMD Millipore	Cat#: 527948
EDTA	Invitrogen	Cat#: AM9260G
DSS	MP Biomedicals	Cat#: 160110
Alcian blue	Alfa Aesar	Cat#: J60122
Tamoxifen	Sigma-Aldrich	Cat#: T5648
DMSO	ThermoFisher	Cat#: BP231
Percoll	Cytiva	Cat#: 17089101
RPMI-1640	Hyclone	Cat#: SH30255.01
DMEM/F12	Gibco	Cat#: 12634-010
PBS	Corning	Cat#: 21040CV
DNase I	Roche	Cat#: 11284932001
Fetal bovine serum	Gibco	Cat#: SH30071.03HI
Bovine serum albumin	ThermoFisher	Cat#: BP1600-100
1x Hank’s Balanced Salt Solution (HBSS)	ThermoFisher	Cat#: 14170112
Liberase TL	Roche	Cat#: 5401020001
Nuclear Fast Red	Electron Microscopy Sciences	Cat#: 26078-05
Hematoxylin	VWR	Cat#: 95057-844
Eosin	VWR	Cat#: 95057-848
Thiazolyl Blue Tetrazolium Bromide (MTT)	Sigma	Cat#: M2128
NEG-50™ Frozen Section Medium	Epredia	Cat#: 6502
Matrigel Matrix	Corning	Cat#: 356231
IntestiCult™ Organoid Growth Medium (Human)	Stemcell	Cat#: 06010
100x penicillin-streptomycin-glutamine	Gibco	Cat#: 10378016
Penicillin-Streptomycin solution, 100X	Corning	Cat#: 30-002-CI
Gentamicin	Gibco	Cat#: 15750060
L-Glutamine	Corning	Cat#: 25-005-CI
N2	Gibco	Cat#: 17502048
B27	Gibco	Cat#: 17504044
Human R-Spondin-1	R&D Systems	Cat#: 4645-RS
Mouse Wnt-3a	R&D Systems	Cat#: 1324-WN
Mouse Noggin	R&D Systems	Cat#: 1967-NG
Human EGF	R&D Systems	Cat#: 236-EG
Mouse EGF	Peprotech	Cat#: 315-09
Human IGF-1	BioLegend	Cat#: 590908
Human FGF-basic	Peprotech	Cat#: 100-18B
N-acetylcysteine	Sigma-Aldrich	Cat#: A9165

REAGENT or RESOURCE	SOURCE	IDENTIFIER
Gastrin-Leu15	Sigma-Aldrich	Cat#: G9145
A83-01	Torics	Cat#: 2939
Y-27632	Sigma-Aldrich	Cat#: Y05030
Cell Recovery Medium	Corning	Cat#: 354253
Gentle Cell Dissociation Reagent	Stemcell	Cat#: 100-0485
TrypLE express	Gibco	Cat#: 12605010
Leukocyte Activation Cocktail, with BD GolgiPlug	BD Biosciences	Cat#: 550583
IC Fixation Buffer	eBioscience	Cat#: 00-8222-49
10x Permeabilization Buffer	eBioscience	Cat#: 00-8333-56
RNA Clean & Concentrator -5 kit	Zymo Research	Cat#: R1015
NEBNext rRNA Depletion Kit	NEB	Cat#: 6310
NEBNext Ultra II Directional RNA Library Prep Kit	NEB	Cat#: 7760
Bioanalyzer High Sensitivity DNA Analysis	Agilent	Cat#: 5067-4626
2-mercaptoethanol	Sigma-Aldrich	Cat#: M6250
Sodium dodecyl sulfate (SDS)	Sigma-Aldrich	Cat#: 436143
16% paraformaldehyde	Electron Microscopy Sciences	Cat#: 15710-S
Sucrose	Sigma-Aldrich	Cat#: S0389
Triton X-100	Sigma-Aldrich	Cat#: T8787
Tween-20	VWR	Cat#: 0777
2-methylbutane	Sigma-Aldrich	Cat#: M32631
CHIR99021	Tocris Bioscience	Cat#: 4423
Deposited data		
ScRNA-seq data: C57BL/6J mouse-derived small intestinal organoids	Gene Expression Omnibus	Accession#: GSE159423
RNA-seq data: terminal ileum of *Il17ra*$^{fl/fl}$*;Atoh1-cre* mice at 6 days post 2.5% DSS treatment	Gene Expression Omnibus	Accession#: GSE189219
Experimental Models: Cell lines		
L-WRN cells	Dr. Thaddeus Stappenbeck Washington University in St. Louis	N/A
Experimental Models: Organisms/Strains		
Mouse: *Villin-cre*	Jackson Laboratory	Cat#: 004586
Mouse: *Villin-cre*^{ERT2}	Dr. Sylvie Robine, Institut Curie-CNRS	Cat#: 020282
Mouse: *ROSA-CAG-LSL-tdTomato*	Jackson Laboratory	Cat#: 007905
Mouse: *Atoh1-cre*	Jackson Laboratory	Cat#: 011104
Mouse: *Atoh1-cre*$^{ER-T2/flox}$*;Rosa*^{Tdtomato}	Dr. Steve Maricich University of Pittsburgh	N/A
Mouse: Atoh1-EGFP	Jackson Laboratory	Cat#: 013593
Mouse: *Defa6-cre*	Dr. Rich Blumberg Harvard University	N/A
Mouse: *Lgr5-EGFP-cre*^{ERT2}	Jackson Laboratory	Cat#: 008875

REAGENT or RESOURCE	SOURCE	IDENTIFIER
Mouse: *Il17ra*$^{fl/fl}$	Dr. Jay Kolls, Tulane University	N/A
Mouse: *Il17ra*$^{-/-}$	Amgen Dr. Jay K. Kolls, Tulane University	N/A
Mouse: *Il17c*$^{-/-}$	Dr. Sarah Gaffen, University of Pittsburgh	N/A
Mouse: *Il17re*$^{-/-}$	Dr. Sarah Gaffen, University of Pittsburgh	N/A
Mouse: *Myd88*$^{fl/fl}$*;Villin-cre*	Dr. Jeremy McAleer, Marshall University	N/A
Mouse: *Lgr5-EGFP-cre*^{ERT2}*; ROSA-CAG-LSL-tdTomato*	Dr. Vincent Yang, Stony Brook University	N/A
Mouse: *Rorc*$^{-/-}$	Dr. Jay K. Kolls, Tulane University	N/A
Oligonucleotides		
Primer Sequences for qPCR-See table 2	This paper	N/A
Mki67 (Mm_Mki67_1_SG)	Qiagen	Cat#: QT00247667
Il17a (Mm00439618_m1)	Applied Biosystems	Cat#: 4331182
Il22 (Mm00444241_m1)	Applied Biosystems	Cat#: 4331182
Hprt (Mm00446968_m1)	Applied Biosystems	Cat#: 4331182
Atoh1 (Mm00476035_s1)	Applied Biosystems	Cat#: 4331182
Chga (Mm0051431_m1)	Applied Biosystems	Cat#: 4331182
Dclk1 (Mm00444950_m1)	Applied Biosystems	Cat#: 4331182
Lgr5 (Mm00438890_m1)	Applied Biosystems	Cat#: 4331182
Muc2 (Mm.PT.58.53535475.g)	IDT	N/A
Tnfa (Mm.PT.58.12575861)	IDT	N/A
Lyz1 (Mm.PT.58.7374112)	IDT	N/A
Clca1 (Mm.PT.58.41915855)	IDT	N/A
Il17ra (Mm.PT.58.17281196)	IDT	N/A
Il17rc (Mm.PT.58.29101252)	IDT	N/A
Software and Algorithms		
Prism 7	GraphPad Software	https://www.graphpad.com/scientificsoftware/prism/
ImageJ	NIH	https://imagej.nih.gov/ij/index.html
cellSens Standard	Olympus	https://www.olympus-lifescience.com/en/software/cellsens/
LSM Image Browser	Zeiss	https://www.embl.de/eamnet/html/body_image_browser.html